arXiv:cond-mat/0109200v1 [cond-mat.soft] 11 Sep 2001

Recent MD Results on Supercooled Thin Polymer Films

F. Varnik[1]*, J. Baschnagel[2], K. Binder[1]

[1] *Institut für Physik, Johannes-Gutenberg Universität, D-55099 Mainz, Germany*
[2] *Institut Charles Sadron, 6 rue Boussingault, F-67083, Strasbourg Cedex, France*

Abstract

The dynamic and static properties of a supercooled (non-entangled) polymer melt are investigated via molecular dynamics (MD) simulations. The system is confined between two completely smooth and purely repulsive walls. The wall-to-wall separation (film thickness), D, is varied from about 3 to about 14 times the bulk radius of gyration. Despite the geometric confinement, the supercooled films exhibit many qualitative features which were also observed in the bulk and could be analyzed in terms of mode-coupling theory (MCT). Examples are the two-step relaxation of the incoherent intermediate scattering function, the time-temperature superposition property of the late time α-process and the space-time factorization of the scattering function on the intermediate time scale of the MCT β-process. An analysis of the temperature dependence of the α-relaxation time suggests that the critical temperature, T_c, of MCT decreases with D. If the confinement is not too strong ($D \geq 10$ monomer diameter) the static structure factor of the film coincides with that of the bulk when compared for the same distance, $T - T_c(D)$, to the critical temperature. This suggests that $T - T_c(D)$ is an important temperature scale of our model both in the bulk and in the films.

PACS: 61.20.Ja,61.25.Hq,64.70.Pf

contribution to *EPJE Special Issue on Properties of Thin Polymer Film*
(guest editor: James Forrest)

Typeset using REVTEX

*To whom correspondence should be addressed. Email: varnik@mail.uni-mainz.de

I. INTRODUCTION

Glass forming materials have been used by mankind since the very early days of civilization. An example are early ceramics from the neolithic period dating back to 5000 B.C. In addition to conventional glasses like those used for windows, bottles, etc., polymers represent a new class of glassy systems with a large variety of thermal and elastic properties. Due to their (in general) low thermal conductivity, polymers are utilized as protective coatings in (micro-) electronic devices, optical fibres and other thermally fragile materials [1–3]. Furthermore, the high dielectric constant of some polymeric compounds suggests their application as porter of electric circuits, a new field under evolution [4,5]. In all these applications, the polymer is in contact with another material. This gives rise to an interface. It is therefore important to know whether and how the interface alters the properties of the system. In particular, one would like to understand to what extent the glass transition temperature is influenced by the polymer-substrate interactions. Hence, the study of the glass transition in thin polymer films finds a strong motivation from the technological side.

In addition to the technological importance, the study of the glass transition in thin polymer films is also of fundamental interest. It could help to elucidate the nature of this phenomenon. According to Adam and Gibbs [6], structural relaxation near the glass transition can take place only if many particles move in a correlated way to allow a collective rearrangement. The average size of such a "cooperatively rearranging region" defines a dynamic correlation length ξ. The larger ξ, the smaller the probability of a cooperative motion and thus the longer the structural relaxation time are supposed to be. If one assumes that ξ diverges at some temperature (Vogel-Fulcher-Tammann temperature) below $T_{\rm g}$, the glass transition can be considered as a thermodynamic second order phase transition.

However, the cooperatively rearranging regions are not directly correlated with static density fluctuations. The structure of a glass former changes only slightly upon cooling contrary to the hypothesized strong increase of ξ. As a consequence, scattering experiments cannot be used to determine $\xi(T)$ [7]. One has to resort to indirect investigations. A possibility consists in studying confined systems. If the system size, L, is finite, one could expect that the cooperatively rearranging region cannot grow beyond any bound, its largest extension being $\xi = L < \infty$. Therefore, the glass transition temperature should depend on L and decrease with system size.

In thin polymer films it is the film thickness, D, which is finite and thus one expects $T_{\rm g} = T_{\rm g}(D)$. Indeed, one finds a dependence of $T_{\rm g}$ on D in both experiments [8–13] and computer simulations [14]. However, the observed change of $T_{\rm g}$ with D strongly depends on the system under consideration. If the interaction between the polymers and the substrate is attractive, the glass transition temperature of the films becomes larger than the bulk value for small film thicknesses [10]. Intuitively, this effect can be attributed to chains which are close enough to the substrate to 'feel' the attractive interaction. The motion of these chains should be slowed down with respect to the bulk. In a thin film almost all chains touch the attractive substrate. So, $T_{\rm g}$ should increase.

On the other hand, measurements (by ellipsometry) of polystyrene (PS) films (of rather large molecular weights) on a silicon substrate showed a significant decrease of $T_{\rm g}$ from 375 K down to 345 K for the smallest film thickness of 10 nm, i.e., a relative change of 10% in $T_{\rm g}$ was observed [9]. There have also been many experiments in recent years on freely

standing polystyrene films (i.e., no solid substrate, but two polymer-air interfaces) [8,11–13] exhibiting a dramatic decrease of T_g by up to 20% if the film thickness becomes much smaller than the chain size. An interesting explanation of this observation in terms of an interplay between polymer-specific properties and free-volume concepts has been proposed [15].

This sensitive dependence of T_g on the polymer-substrate interaction was also obtained from computer simulations [14]. One finds that a strongly attractive wall leads to an increase of T_g, whereas a weaker attraction has the opposite effect. Therefore, for repulsive walls, a decrease of T_g can be expected, provided that other parameters of the system, in particular the average density, are unaffected by the confinement. As the simulations of our system in the bulk were done at constant external pressure [16,17], we also carried out the simulations of the films at constant normal pressure in order to obtain an average density that lies as close as possible to the bulk density at the same temperature. This allows to separate the effect of confinement from that of the density.

Note however that the glass transition temperature is an empirical quantity. It is usually defined as the temperature at which the viscosity reaches a value of 10^{13} poise. So, the choice of another number would give a different value of T_g. Furthermore, T_g depends on the cooling rate so that it is not a temperature in a strict thermodynamic sense. Therefore, other temperatures have been introduced to characterize the glass transition. One example is the so-called Vogel-Fulcher-Tammann (VFT)-temperature, T_0, at which the system viscosity seems to diverge. This quantity is obtained by fitting the viscosity, $\eta(T)$, to the empirical function, $\eta(T) = \eta_0 \exp[E/(T - T_0)]$. An attempt to rationalize the VFT-law is the free volume theory [18–21]. The main idea of this approach is that a tagged particle can leave its initial position only if it finds a "free volume" of size $v_f \geq v_c$ in its neighborhood (v_c being some critical volume of the order of the size of a molecule). It is further supposed that the average free volume vanishes at T_0. Assuming statistical independence of the free volumes and using a Taylor expansion of the average free volume around T_0, one obtains the VFT-law for transport coefficients like the viscosity or the (inverse) diffusion coefficient. This brief description illustrates that the free volume theory has a phenomenological character. The precise meaning of the free volume is unclear and the existence of T_0, where v_f is supposed to vanish, is not derived, but postulated.

Contrary to the VFT-temperature, the critical temperature of the so-called mode-coupling theory (MCT) results from a microscopic approach to the dynamics of supercooled (simple) liquids [22–24]. Within the idealized version of the theory, the structural relaxation time diverges at a critical temperature T_c, while the static properties of the system remain liquid-like. This implies that the system vitrifies at T_c. Thus, from the point of view of MCT, the glass transition is a purely dynamic phenomenon. However, comparisons between the theory and experiments [24,25] reveal that T_c lies in the region of the supercooled liquid, where the glass former is only moderately viscous and no absolute freezing occurs. In reality, there are additional relaxation mechanisms which are not incorporated in the idealized MCT and begin to dominate close to and especially below T_c. An attempt was made to approximately include these relaxation processes in an extended version of MCT [23], but the validity of this extension is currently unclear [26]. Nevertheless, the idealized MCT derives several empirically known phenomena, such as the stretching of the α-relaxation, which is often described by the Kohlrausch-Williams-Watts (KWW)-law ($\propto \exp[-(t/\tau)^\beta]$, where $\beta < 1$), or the time-temperature superposition principle. Furthermore, it also makes

new predictions, such as the space-time factorization property, which have been tested both in experiments [24,25] and computer simulations [27].

An application of MCT to our polymer model in the bulk [17,28–31] revealed that the theory represents a suitable framework to analyze the dynamics of the supercooled melt. Therefore, we attempt to test whether MCT can also be applied to the supercooled polymer films. We find that even for an extremely thin film of three monomer layers, some features of the dynamics at low temperatures can be successfully described by the MCT. This analysis yields T_c as a function of film thickness and shows that T_c decreases with D. Within the error bars the Vogel-Fulcher-Tammann temperature exhibits the same D-dependence so that we also expect the glass transition temperature of our model to behave analogously due to $T_0(D) \leq T_g(D) \leq T_c(D)$.

The paper is organized as follows: After a presentation of the model in section II, section III focuses on the influence of the confinement on static properties of the system. A discussion of the dynamics is the subject of section IV. In section V we determine the dependence of T_c and T_0 on film thickness and the last section summarizes our conclusions.

II. MODEL

We study a Lennard-Jones (LJ) model for a dense polymer melt [16,32] of short chains (each consisting of 10 monomers) embedded between two completely smooth, impenetrable walls [33,34]. Two potentials are used for the interaction between particles. The first one is a truncated and shifted LJ-potential which acts between all pairs of particles regardless of whether they are connected or not,

$$U_{\text{LJ-ts}}(r) = \begin{cases} U_{\text{LJ}}(r) - U_{\text{LJ}}(r_c) & \text{if } r < r_c \ , \\ 0 & \text{otherwise} \ , \end{cases}$$

where $U_{\text{LJ}}(r) = 4\epsilon\Big[(\sigma/r)^{12} - (\sigma/r)^6\Big]$ and $r_c = 2 \times 2^{1/6}\sigma$. The connectivity between adjacent monomers of a chain is ensured by a FENE-potential [32],

$$U_{\text{FENE}}(r) = -\frac{k}{2}R_0^2 \ln\left[1 - \left(\frac{r}{R_0}\right)^2\right] , \tag{1}$$

where $k = 30\epsilon/\sigma^2$ is the strength factor and $R_0 = 1.5\sigma$ the maximum allowed length of a bond. The wall potential was chosen as

$$U_{\text{W}}(z) = \epsilon\left(\frac{\sigma}{z}\right)^9 , \tag{2}$$

where $z = |z_{\text{particle}} - z_{\text{wall}}|$ ($z_{\text{wall}} = \pm D/2$). This corresponds to an infinitely thick wall made of infinitely small particles which interact with inner particles via the potential $45\epsilon(\sigma/r)^{12}/(4\pi\rho_{\text{wall}}\sigma^3)$ where ρ_{wall} denotes the density of wall particles. The sum over the wall particles then yields $\epsilon(\sigma/z)^9$. All simulation results are given in Lennard-Jones (LJ) units. All lengths and energies are measured respectively in units of σ and ϵ, temperature in units of ϵ/k_B ($k_B = 1$) and time in units of $(m\sigma^2/\epsilon)^{1/2}$.

The left panel of Fig. 1 compares the bond potential, i.e. the sum of LJ- and FENE-potentials, with the LJ-potential. It shows that the bonded monomers prefer shorter distances than the non-bonded ones. Thus, our model contains two intrinsic length scales (see right panel of Fig. 1 for a schematic illustration). Since these length scales are chosen to be incompatible with a (fcc or bcc) crystalline structure and since our chains are flexible (no bond angle or torsion potentials), one could expect that the system does not crystallize at low temperatures, but remains amorphous [35].

This expectation is well borne out, as Fig. 2 illustrates. The upper part of the figure shows a snapshot of a film of thickness $D=20$ and at temperature $T=0.44$ which corresponds to the supercooled state. The visual inspection of this configuration suggests that the structure is disordered. This is corroborated by an analysis of the static structure factor $S(q)$.

The lower part of Fig. 2 shows $S(q)$ for a film of thickness $D=10$ at temperatures corresponding to the normal liquid state and to the supercooled state. $S(q)$ is calculated parallel to the walls [i.e. $q=|\boldsymbol{q}|$, $\boldsymbol{q}=(q_x,q_y)$] by averaging over all monomers in the system. Figure 2 shows that the maximum value of the $S(q)$ increases at lower temperature and that its position is slightly shifted towards larger q-values. Thus, the average interparticle distance decreases with decreasing temperature, since the density of the film increases in our simulations at constant pressure [34]. However, these structural changes are rather small. Even at a very low temperature of $T=0.42$ which is quite close to the critical temperature of the system at this film thickness ($T_{\rm c}(D=10)\simeq 0.39$), *no qualitative difference* is observed between the structure factors at low and high temperatures. The packing of the system thus remains liquid-like (i.e. amorphous) at all studied temperatures.

All simulations have been carried out at constant normal pressure $P_{\rm N,ext}=p=1$ [34]. However, to adjust the normal pressure, we do *not* vary the wall-to-wall separation, D, but the surface area. For each temperature, the average surface area is calculated by an iterative approach [36]. The system is then propagated until the instantaneous surface area reaches the computed average value. At this point the surface area (and thus the volume) is fixed and a production run is started in NVT-ensemble, where the temperature is adjusted using the Nosé-Hoover thermostat [37,38]. This thermostat slows down or accelerates all particles depending on the sign of the difference between the instantaneous kinetic energy of the system and the desired value imposed, i.e. $3Nk_{\rm B}T/2$ (N is the number of particles) [37–42].

One may therefore ask how reliable the resulting dynamics is when compared to pure Newtonian dynamics in the microcanonical (NVE) ensemble. This question was already examined for the bulk system in Ref. [16] and for our confined model in Refs. [43,44]. In both cases, the results obtained from constant energy (NVE) simulations and from the Nosé-Hoover thermostat are identical. More details about the applied simulation techniques can be found in [34,36,44].

III. STATIC PROPERTIES

In this section, we want to discuss the influence of confinement on both the chain conformation and the static properties of the melt. When computed within thin layers parallel to the wall, the structure of a chain varies with the distance from the wall. On the other hand, the chain structure averaged over the whole film does not depend much on film thickness.

Contrary to this insensibility of the average chain conformation to the confinement, the dense packing of the melt exhibits a pronounced dependence on D.

A. Effects of the Confinement on the Structure of a Chain

Let us first look at the T-dependence of the single chain structure factor $S^{\rm c}(q)$. Similarly to $S(q)$, $S^{\rm c}(q)$ is also calculated for q-vectors in direction parallel to the walls and by averaging over all chains in the system.

The upper panel of Fig. 3 shows $S^{\rm c}(q)$ for a film of thickness $D=20$ at two representative temperatures: a relative high temperature corresponding to the normal liquid state ($T=1$) and a low temperature representative of the supercooled state ($T=0.44$). Contrary to the structure factor of the melt (see Fig. 2), $S^{\rm c}(q)$ is practically independent of the temperature, not only on scales larger than the radius of gyration, but also on the local scale of the intermonomer distance. This may be rationalized as follows: The interactions of the monomers along the backbone of a chain do not include specific potentials for the bond or torsional angles, which could make the chain expand with decreasing temperature. This would lead to a much stronger temperature dependence than that resulting from potentials used. Since the bond potential is very steep around the minimum and is in general very large, the bond length is essentially independent of T ($b=\sqrt{\langle \boldsymbol{b}\cdot\boldsymbol{b}\rangle}=0.966$ at $T=1$, $b=\sqrt{\langle \boldsymbol{b}\cdot\boldsymbol{b}\rangle}=0.961$ at $T=0.46$. Here, $\boldsymbol{b}$ is the bond vector). The main effect is that the overall size of a chain slightly shrinks with decreasing temperature because the density increases. This also leads to a weak increase of the peak of $S^{\rm c}(q)$ at $q=7.6$, which is, however, not visible on the scale of Fig. 3 and negligible compared to that of $S(q)$ in Fig. 2.

Furthermore, Fig. 3 shows that, for $q \le 2\pi/R_{\rm g}^{\rm bulk}$, the q-dependence of $S^{\rm c}(q)$ can be described well by a Debye-function,

$$S^{\rm Debye}(q)=\frac{2N_{\rm p}}{(q^2R_{\rm g}^{2\ {\rm Debye}})^2}\Big(\exp(-q^2R_{\rm g}^{2\ {\rm Debye}})-1+q^2R_{\rm g}^{2\ {\rm Debye}}\Big)\ , \qquad (3)$$

with $R_{\rm g}^{2\ {\rm Debye}}=R_{\rm g}^{2\ {\rm bulk}}$, where $R_{\rm g}^{2\ {\rm bulk}}$ was calculated independently and inserted in Eq. (3) [$N_{\rm p}$ is the number of the monomers of a chain (degree of polymerization)]. The same observation has already been made for the model in the bulk [16]. This agreement may be expected because the scattering for $q \le 2\pi/R_{\rm g}^{\rm bulk}$ is determined by the overall size of a chain. On this scale, the difference between the freely-jointed chain model utilized to derive the Debye function and the actual model of the simulation does not matter.

The lower panel of Fig. 3 shows $S^{\rm c}(q)$ for films of various thicknesses D at $T=1$. Obviously, the chain conformation averaged over the whole film does not depend much on D. Contrary to the small effect of temperature on $S^{\rm c}(q)$, the independence of film thickness is less intuitive. Figure 4 illustrates this point. In the upper panel we compare the parallel and perpendicular components of the radius of gyration and of the end-to-end distance, $R_{{\rm g},\parallel}^2$, $R_{{\rm g},\perp}^2$ and $R_{{\rm ee},\parallel}^2$, $R_{{\rm ee},\perp}^2$, for $D=20$ and $T=1$ (normal liquid phase). The components are plotted versus the distance, z, from the (left) wall, where z denotes the position of chain's center of mass. So, $R_{{\rm g},\parallel}^2(z)$, for instance, is the radius of gyration parallel to the wall, which is averaged over all chains whose centers of mass are located at z. The figure shows that both the radius of gyration and the end-to-end distance agree with the bulk value if

$z > z_w + 2R_g^{bulk}$. Here, $z_w \approx 1$ denotes the physical position of the wall, i.e., the smallest distance between a monomer and $z_{wall} = D/2$. As the chain's center of mass approaches the wall, $R^2_{g,\parallel}$ and $R^2_{ee,\parallel}$ first develop a shallow minimum and then increase to about twice the bulk value followed by a sharp decrease to zero in the very vicinity of the wall where practically no chain is present. On the other hand, the perpendicular components, $R^2_{g,\perp}$ and $R^2_{ee,\perp}$, first pass through a maximum before decreasing to almost 0 at the wall. This behavior has been observed in several other simulations (see [45] and references therein), also for larger chain length than that used here [46,47].

These results suggest that a spatially resolved version of the chain structure factor, $S^c(q,z)$, should depend upon the position of the chain with respect to the wall. To test this idea we divide the system into layers of thickness 1/4 (in units of σ which roughly corresponds to the monomer diameter) and evaluate $S^c(q,z)$ by taking into account all monomer pairs within the layer which belong to the same chain. Here, z is the distance of the middle of such a layer from the wall. The lower panel of Fig. 4 shows $S^c(q,z)$ for an extremely thin film of thickness $D=5$ at $T=0.35$ and for two typical layers: a layer in the film center ($z=2.375$) and a layer close to the wall ($z=1.125$) [note that all layers with a distance smaller than $z=1.125$ to the wall are practically empty. Note also that there is no layer whose middle lies exactly in the film center $z=2.5$. Only the boundary of the central layer "touches" the film center so that its middle is closer to the wall than $D/2=2.5$]. In the center of the film $S^c(q,z)$ can be described by a Debye function with $R_g^{2\ \mathrm{Debye}} = 1.93$, whereas a larger radius ($R_g^{2\ \mathrm{Debye}} = 2.4$) must be chosen close to the walls. These values for $R_g^{2\ \mathrm{Debye}}$ are taken from the profile of the radius of gyration for $D=5$ at $T=0.35$, which yields $R_g^2 = 2.4$ and $R_g^2 = 1.93$ when averaging over the intervals $1 \le z \le 1.25$ and $2.25 \le z \le 2.5$, respectively. Furthermore, Fig. 4 shows that $S^c(q,z)$ for the film center coincides with $S^c(q)$ obtained by averaging over the whole system. Thus, the local variations of $S^c(q,z)$ close to the wall disappear when the whole system is considered. Qualitatively, this point can be understood by noting that there are only few chains close to the wall, where $R^2_{g,\parallel}(z)$ is larger than the bulk value, while most of chains are in the inner part of the film, where $R^2_{g,\parallel}(z)$ is close to $R_g^{2\ \mathrm{bulk}}$. Averaging over the whole system thus tends to cancel the effects of the walls on the chain conformation.

This point is further examined in Fig. 5. The upper panel of the figure shows $1.5R^2_{g,\parallel}$, $3R^2_{g,\perp}$, averaged over the whole film, and $R_g^2 = R^2_{g,\parallel} + R^2_{g,\perp}$ versus temperature for two film thicknesses $D=5$ and $D=20$. For all temperatures the parallel component is larger than the bulk value, whereas the perpendicular one is smaller. The disparity between the two components becomes more pronounced for small film thickness. Nevertheless, the sum of these quantities, R_g^2, is fairly close to the bulk value for both film thicknesses. It slightly shrinks with decreasing temperature, since the density of the films increases. Similar trends are observed if D is varied and T is kept constant. The lower panel of Fig. 5 depicts $1.5R^2_{g,\parallel}$, $3R^2_{g,\perp}$ and R_g^2 as a function of film thickness at $T=0.5$. R_g^2 depends only weakly on film thickness and is close to the bulk value. This explains why the chain structure factors of Fig. 3 are essentially independent of D.

B. The Packing Structure of the Melt

Figure 6 compares the structure factor of the melt, $S(q)$, in the bulk with that of films of various thicknesses at $T = 1$ (normal liquid state; upper panel of the figure) and at $T = 0.46$ (supercooled state; lower panel of the figure). Qualitatively, the behavior of the films and the bulk is identical. The structure factor is small at small q-values, reflecting the low compressibility of the system. Then, it increases and develops a peak at $q_{\max}$ which corresponds to the local packing of monomers ($2\pi/q_{\max} \approx 1$) before it decreases again and begins oscillating around 1, the large-q limit of $S(q)$. This behavior is characteristic of dense amorphous packing.

However, there are quantitative differences which become more pronounced at low temperature: While $S(q)$ of the film of thickness $D = 20$ (almost) coincides with the bulk data at $T = 1$, deviations are clearly visible at $T = 46$. Quite generally, the most prominent differences between the bulk and the film are found for small q and for $q_{\max}$. The compressibility of the film is higher, the value of $q_{\max}$ is shifted to slightly lower q and the magnitude of $S(q_{\max})$ is smaller than in the bulk. Keeping the film thickness fixed, one can observe similar changes of $S(q)$ as the temperature increases (see Fig. 2). Therefore, the local packing of the monomers in the films seems to resemble that of the bulk at some higher temperature. Since the local structure of the melt has an important influence on its dynamic behavior in the supercooled state [22], Fig. 6 suggests that the film relaxes more easily than the bulk at the same temperature. Indeed, we will see later that the dynamics of the system is much faster in the film than in the bulk when compared at the same temperature.

IV. DYNAMICS

This section discusses the dynamics of the films at low temperatures and for various thicknesses, D, ranging from about 3 to about 14 times the bulk radius of gyration. To this end, the incoherent intermediate scattering function and various mean-square displacements were calculated. We will see that, despite the geometric confinement, the films exhibit several dynamic features which are in agreement with predictions of mode-coupling theory (MCT) [22–25]. In this respect, the films behave as the bulk [17,28–31]. However, the onset of MCT effects is shifted to lower temperatures compared to the bulk. The presence of the smooth walls accelerates the dynamics and this influence of confinement is the stronger, the smaller D.

A. Confinement leads to Faster Dynamics

An interesting dynamic correlation function is the incoherent intermediate scattering function $\phi_q^{\mathrm{s}}(t)$. It measures density fluctuations on various length scales, which are caused by the displacement of individual particles. For a planar system, we define $\phi_q^{\mathrm{s}}(t)$ for q-vectors parallel to the wall, i.e.,

$$\phi_q^{\mathrm{s}}(t) = \left\langle \frac{1}{N} \sum_{i=1}^{N} \exp\left(\mathrm{i}\boldsymbol{q}_{\parallel} \left[\boldsymbol{r}_{i,\parallel}(t) - \boldsymbol{r}_{i,\parallel}(0) \right] \right) \right\rangle . \tag{4}$$

Here, N is the total number of monomers in the system, $\boldsymbol{q}_\parallel = (q_x, q_y)$, $q = |\boldsymbol{q}_\parallel| = \sqrt{q_x^2 + q_y^2}$ and $\boldsymbol{r}_{i,\parallel} = (x_i, y_i)$.

Figure 7 compares the relaxation of $\phi_q^{\rm s}(t)$ at the maximum of the static structure factor ($q = 6.9$) in the bulk with that in films of various thicknesses ranging from $D = 5 \approx 3.5 R_{\rm g}$ to $D = 20 \approx 14 R_{\rm g}$. The temperature studied, $T = 0.46$, is slightly above $T_{\rm c}^{\rm bulk}$ ($= 0.45$) [17,28–31]. In the bulk, a two-step relaxation is observed: At very short times, $\phi_q^{\rm s}(t)$ can be described by $\phi_q^{\rm s}(t) = 1 - (\Omega_{\rm s} t)^2/2$ with the microscopic frequency $\Omega_{\rm s} = q\sqrt{k_{\rm B}T}$ [22]. This corresponds to free particle motion. At later times, the relaxation of $\phi_q^{\rm s}(t)$ is strongly protracted. There is an intermediate time window (β-relaxation regime of MCT [22]), where the correlator changes rather slowly with time before the final structural relaxation (α-relaxation) sets in at long times. This two-step decay is a characteristic feature of $\phi_q^{\rm s}(t)$ for temperatures close to $T_{\rm c}$ and reflects the temporary "arrest" of a monomer in its local environment ("cage effect" [22]). It has been analyzed in detail in Refs. [16,17,48,49].

Compared to the bulk, the film data relax faster. If the film thickness decreases, this acceleration is enhanced and the two-step decay gradually disappears. At $D = 5$, no intermediate β-relaxation is observed. The same changes also occur in the bulk if the temperature increases [17,29,48]. This suggests that the inverse film thickness qualitatively plays a similar role as the temperature.

The acceleration of the dynamics in the film compared to the bulk is not limited to the main peak of $S(q)$. It is also found for other q-values, for instance, for very small wave vectors. Since the time dependence of $\phi_q^{\rm s}(t)$ is directly related to the monomer mean-square displacement (MSD) in the low-q limit, it is instructive to illustrate the acceleration of the dynamics by an investigation of the MSD. For a polymer system, various kinds of MSD's may be defined. An important example is the mean-square displacement of the innermost monomer,

$$g_1(t) = \frac{3}{2M} \sum_{i=1}^{M} \left\langle [\boldsymbol{r}_{i,\parallel}^{\rm inner}(t) - \boldsymbol{r}_{i,\parallel}^{\rm inner}(0)]^2 \right\rangle \ . \tag{5}$$

Here, M is the total number of chains in the melt and $\boldsymbol{r}_{i,\parallel}^{\rm inner} = (x_i^{\rm inner},\ y_i^{\rm inner})$ is the projection of the position vector of the innermost monomer of the i-th chain onto the xy-plane (which is parallel to the walls). The factor $3/2$ is introduced to simplify the comparison with bulk results. It takes into account that only two independent directions (x and y) contribute to the MSD in the film, whereas all three directions are considered in the bulk[1]. Similarly, one defines the mean-square displacements of the chain's center of mass,

$$g_3(t) = \frac{3}{2M} \sum_{i=1}^{M} \left\langle [\boldsymbol{R}_{i,\parallel}^{\rm cm}(t) - \boldsymbol{R}_{i,\parallel}^{\rm cm}]^2 \right\rangle \ , \tag{6}$$

where $\boldsymbol{R}_{i,\parallel}^{\rm cm}$ is the projection of vector to the i-th chain's center of mass onto a plane parallel

[1] As most of the comparisons with bulk results are done using the film data in parallel direction, we drop the index "$\parallel$" to simplify the notation. To avoid ambiguities, when film data in perpendicular direction are discussed, an index "$\perp$" will then be used.

to the wall. Again, the factor 3/2 accounts for the difference in the number of independent components, as above.

Figure 8 depicts $g_1(t)$ for two typical temperatures: $T = 1$ (upper panel), which corresponds to the normal liquid state, and $T = 0.46$ (lower panel), which belongs to the supercooled state in the bulk. Both panels compare $g_1(t)$ for the bulk and for films of various thicknesses. The influence of the walls is rather small at $T = 1$ so that $g_1(t)$ of the bulk almost overlaps with that of the film if $D \geq 10$. However, the lower panel of Fig. 8 shows that the effect of the walls on the mobility becomes significant at all studied thicknesses with progressive supercooling. Outside the initial ballistic regime ($g_1(t) = 3Tt^2$), the motion resembles that of the bulk, but is the faster, the smaller the film thickness. For the bulk and $D \gtrsim 7$, $g_1(t)$ exhibits several regimes. In agreement with the predictions of the mode-coupling theory [22–24], a plateau regime emerges after the ballistic motion. At low temperature, the tagged particle remains temporarily in the "cage" formed by its neighbors. However, contrary to simple (atomic) liquids, where a direct crossover from the plateau to the diffusive regime occurs, an intermediate subdiffusive regime emerges due to the connectivity of the monomers [50]. In this regime, which is present for all D, the center of mass already crosses over to the asymptotic diffusive motion, $g_3(t) \simeq t$, whereas the motion of the innermost monomer is described by a power law $g_1(t) \sim t^x$ with an effective exponent $x \simeq 0.63$. The innermost monomer reaches the center of mass only if $g_1(t)$ is larger than the end-to-end distance of a chain. In this limit, the diffusive motion is dominated by the motion of the chain's center of mass and $g_1(t)$ coincides with $g_3(t)$.

In addition to the parallel displacements the analysis of the motion perpendicular to the wall is also interesting because the oscillations of the monomer density profile, which can propagate through the whole film for small D and low T, could possibly suppress perpendicular motion substantially. To check that, Fig. 9 shows the MSD of all monomers, $g_0(t)$, computed in direction parallel to wall,

$$g_0(t) = \frac{3}{2N} \sum_{i=1}^{N} \left\langle [\boldsymbol{r}_{i,\parallel}(t) - \boldsymbol{r}_{i,\parallel}]^2 \right\rangle \ , \tag{7}$$

and perpendicular to it

$$g_{0,\perp}(t) = \frac{3}{N} \sum_{i=1}^{N} \left\langle [z_i(t) - z_i(0)]^2 \right\rangle \ . \tag{8}$$

Here, N is again the total number of monomers and $\boldsymbol{r}_{i,\parallel} = (x_i,\ y_i)$. Furthermore, z_i denotes the z position of i-th monomer. The factors 3/2 for $g_0(t)$ and 3 for $g_{0,\perp}(t)$ account for the difference of independent components: two in parallel and one perpendicular direction compared to 3 in a bulk system.

The upper panel of Fig. 9 depicts $g_0(t)$ at $T = 0.46$ (supercooled state). It compares the bulk data with the displacements parallel and perpendicular to the walls in films of thicknesses $D = 5,\ 7$ and 20. The comparison of $g_{0,\perp}(t)$ for the films and of $g_0(t)$ for the bulk reveals that the confinement does not only accelerate the dynamics in parallel, but also in perpendicular direction if $g_{0,\perp}(t, D)$ is sufficiently smaller than the film thickness. For all D, one then finds $g_{0,\perp}(t, D) > g_0^{\text{bulk}}(t)$ and $g_{0,\perp}(t, D_1) > g_{0,\perp}(t, D_2)$ if $D_1 < D_2$. However, this

increase of the mobility is less pronounced than that of the dynamics in parallel direction, so that, for a given film thickness, $g_{0,\parallel}(t, D) > g_{0,\perp}(t, D)$.

Of course, the perpendicular displacement cannot grow infinitely. It must be limited by the film thickness. This is illustrated by $g_{0,\perp}(t, D=5)$ which crosses over to a constant of approximately 5 at late times. In fact, using the density profile, $\rho(z)$, one can compute the large time limit of $g_{0,\perp}(t)$ by

$$\lim_{t\to\infty} g_{0,\perp}(t) = 3\,\frac{\displaystyle\int_{-D/2}^{+D/2} \mathrm{d}z \int_{-D/2}^{+D/2} \mathrm{d}z' \rho(z)\rho(z')(z-z')^2}{\Big(\displaystyle\int_{-D/2}^{+D/2} \rho(z)\mathrm{d}z\Big)^2}\,. \tag{9}$$

Equation (9) can be understood as follows: The contribution of two points z and z' to the long time limit of $g_{0,\perp}(t)$ is equal to $(z-z')^2$ multiplied by the probability $p^{(2)}(z,t;\,z',t')\,\mathrm{d}z\,\mathrm{d}z'$ of finding a tagged particle at a given time, t', in the interval $[z', z'+\mathrm{d}z']$ provided that it was at a previous time, t in $[z, z+\mathrm{d}z]$. As $|t-t'|$ grows, this probability becomes independent of the initial position of the particle, i.e. $p^{(2)}(z,t;\,z',t') = p(z,t)\,p(z',t')$, where $p(z,t)\,\mathrm{d}z$ is the probability of finding a particle at time t in $[z, z+\mathrm{d}z]$. Obviously, this probability does not depend on the choice of the time origin, i.e. $p(z,t) = p(z) = \rho(z)/\int \rho(z')\mathrm{d}z'$. Putting all this together and adding a factor of 3 for the sake of comparison with bulk results, we obtain $3(z-z')^2\rho(z)\,\rho(z')\,\mathrm{d}z\mathrm{d}z'/(\int \rho(z)\mathrm{d}z)^2$ for the contribution of the pair (z, z') to $\lim_{t\to\infty} g_{0,\perp}(t)$. Integration over both variables z and z' yields Eq. (9).

For a film of thickness $D = 5$ at a temperature of $T = 0.46$ insertion of the density profile (obtained from the simulation) in Eq. (9) yields $\lim_{t\to\infty} g_{0,\perp}(t) = 4.667$. This is the value to which $g_{0,\perp}(t, D = 5)$ converges for large t (Fig. 9). Note that by replacing the monomer density profile $\rho(z)$ in Eq. (9) by the density profile of the innermost monomer, one can obtain the long time limit of $g_{1,\perp}(t)$, i.e. $g_{1,\perp}(t=\infty)$. In a similar way, Eq. (9) can be adapted to compute $g_{4,\perp}(t=\infty)$ by using the density profile of end monomers and/or $g_{3,\perp}(t=\infty)$ by replacing $\rho(z)$ by the profile of the density of the chain's center of mass, $\rho_{\mathrm{cm}}(z)$.

The general validity of Eq. (9) is demonstrated in the lower panel of Fig. 9. Here, $g_{0,\perp}(t)$ and $g_{1,\perp}(t)$ are plotted for two temperatures, $T=0.46$ and $T=1$. The corresponding long time limits have been computed as discussed above. At both temperatures the results obtained by Eq. (9) are in good agreement with long time behavior of $g_{0,\perp}(t)$ and $g_{1,\perp}(t)$. The inset of the lower panel of Fig. 9 depicts the density profiles of all monomers and of the innermost monomer at both investigated temperatures. As seen from this inset, the density close to the walls increases appreciably at lower temperatures. Furthermore, the formation of strong density peaks close to the walls is accompanied by a slight decrease of the density in the center of the film. As a consequence, the relative weight of larger transversal distances in Eq. (9) increases compared to that of smaller $(z - z')$. One can therefore expect an increase of $g_{0,\perp}(t=\infty)$ at lower T. As the density of the innermost monomer changes in a similar way with temperature, we also expect an increase of $g_{1,\perp}(t=\infty)$ when decreasing T. This expectation is nicely born out in the lower panel of Fig. 9.

B. Incoherent intermediate scattering function

The discussion of the previous sections suggested that mode-coupling theory (MCT) could also be a relevant theoretical framework to describe the dynamics of the supercooled polymer films. In this section we want to test this suggestion by an analysis of the incoherent intermediate scattering function $\phi_q^{\rm s}(t)$.

A quantitative application of MCT to the simulation data requires an intricate fit procedure which must simultaneously optimize several parameters subject to various theoretical constraints (some of them have to be independent of temperature, others independent of the wave vector). Before attempting this analysis simple tests should be carried out to check whether the approach is worthwhile at all. Two such tests can be performed.

Mode-coupling theory predicts that there is an intermediate time window in which the scattering function remains close the time- and temperature independent non-ergodicity parameter $f_q^{\rm sc}$. This time window is called β-relaxation regime [22,25]. In this regime the scattering function can be written as

$$\phi_q^{\rm s}(t) = f_q^{\rm sc} + h_q^{\rm s} G(t) \; , \tag{10}$$

where $G(t)$ and $h_q^{\rm s}$ are the β-correlator and the critical amplitude, respectively [22,25]. Equation (10) shows that the time-dependent corrections to $f_q^{\rm sc}$ have an important property. The space- and the time dependences factorize from one another.

This "factorization theorem" [22,25] suggests a simple test [48,49,51,52] which uses the simulation data directly without invoking any fit procedure. If t' and t'' denote two times belonging to the β-regime, then the ratio

$$R_q^{\rm s}(t) = \frac{\phi_q^{\rm s}(t) - \phi_q^{\rm s}(t')}{\phi_q^{\rm s}(t'') - \phi_q^{\rm s}(t')} = \frac{G(t) - G(t')}{G(t'') - G(t')} = R(t) \tag{11}$$

should only depend on temperature and time, but not on q, provided Eq. (10) holds.

Note that $\phi_q^{\rm s}(t)$ varies slowly for times around the plateau. Therefore, the denominator of Eq. (11) is fairly small and the accuracy of the test is predicated upon an appropriate choice of the parameters t'' and t'. To obtain a satisfactory signal-to-noise ratio, one would like to make t'' and t' as different as possible. However, one has to be careful not to take t'' and t' outside the β-relaxation regime, where Eq. (11) is no longer valid. We find that $t''=1$ and $t'=50$ is a reasonable compromise for all studied film thicknesses $D=5$, 10 and $D=20$.

With this choice two observations can be made from Fig. 5: First, there is indeed an intermediate time window for all D where the correlators, measured at different q, collapse, whereas they splay out at both shorter and longer times. This is a qualitative evidence for the factorization theorem. However, the best agreement with Eq. (11) is obtained for $D=10$. In the other two cases the superposition of the scattering functions for $t'' < t < t'$ is not as good. A possible reason for this difference could be that, for $D=10$, Eq. (11) is tested at a distance of $T - T_{\rm c}(D=10) = 0.42 - 0.39 = 0.03$ from the critical temperature of this film thickness. The tests for $D=20$ and $D=5$, however, correspond to $T - T_{\rm c}(D=20) = 0.46 - 0.415 = 0.045$ and $T - T_{\rm c}(D=5) = 0.35 - 0.305 = 0.045$, respectively. As Eq. (11) is an asymtotic relation which is expected to hold the better, the closer T is to $T_{\rm c}$, Fig. 5 still suggests that the factorization theorem is not only satisfied in the bulk [17,48], but also in the polymer films.

The second observation concerns the order of the q-values before and after the β-regime. This order is preserved. The top curve, $\phi^{\rm s}_{q=1}(t)$, at short times is also the top curve in the α-regime. Similarly, the bottom curve, $\phi^{\rm s}_{q=18.5}(t)$, before the β-regime also remains below all other q-values when leaving the β-regime again. This behavior reflects the theoretical prediction that the short- and long-time corrections to Eq. (10) exhibit the same q-dependence. It was pointed out in simulations of a binary Lennard-Jones mixture [52] and also found for our model in the bulk [48].

The second test of the applicability of MCT deals with the late-time relaxation of $\phi^{\rm s}_q(t)$. An important prediction of the theory for the α-process is the time-temperature superposition principle (TTSP) [22,25]. This means that $\phi^{\rm s}_q(t)$ is not a function of time and temperature separately, but only of the scaled time $t/\tau_q(T)$, where $\tau_q(T)$ is the α-relaxation time. So, we have

$$\phi^{\rm s}_q(t) = F_q(t/\tau_q) \; . \tag{12}$$

The function $F_q(t/\tau_q)$ can often be well approximated by a Kohlrausch-Williams-Watts (KWW) function

$$F_q(t/\tau^{\rm K}_q) = f^{\rm K}_q \exp\left[(t/\tau^{\rm K}_q)^{\beta^{\rm K}_q}\right] . \tag{13}$$

For time-temperature superposition to hold the amplitude $f^{\rm K}_q$ and the stretching exponent $\beta^{\rm K}_q$ must be independent of temperature. Only the Kohlrausch relaxation time $\tau^{\rm K}_q$ is a function of T. MCT predicts that $\tau^{\rm K}_q$ is proportional to the α-relaxation time and increases upon cooling as [22,25]

$$\tau^{\rm K}_q \propto \tau_q \sim (T - T_{\rm c})^{-\gamma} \; . \tag{14}$$

Equation (14) also implies that any time from the window of the α-process should exhibit the same temperature dependence and can thus be used to test the TTSP. This means that it should be possible to collapse the late time decay of the scattering functions, measured at different T, onto a common T-independent master curve by plotting $\phi^{\rm s}_q(t)$ versus t/τ_q. A convenient definition of τ_q is to simply read off the time when $\phi^{\rm s}_q(t)$ has decay to a certain value. Again, such a test has the advantage that no complicated fit procedure is involved. It works directly with the simulation data. A possible choice is $\phi^{\rm s}_q(\tau_q) = 0.1$ [49]. This low value warrants that the scattering function has decayed sufficiently so that possible perturbations from the β-relaxation are completely negligible.

The resulting master curves are shown in Fig. 11 for $D = 5, 10, 20$. For all film thicknesses, even for the extreme case of $D = 5$, which corresponds to three atomic layers only, the TTSP is borne out by the simulation data and extends to shorter rescaled times with decreasing temperature, as predicted by MCT for homogeneous systems. In this respect, the films behave identical to the bulk [17,49]. However, the results for $D = 10$ suggest that there could also be a qualitative difference. They include $T = 0.4$, which is very close to the estimated $T_{\rm c}$, i.e. $T - T_{\rm c} = 0.01$. Contrary to the bulk [17,49], the film data at this $T - T_{\rm c}$ exhibit no apparent violation of the TTSP. Whether this is a general property of the confined systems or just a special feature of $D = 10$ is not clear at present.

While the scattering functions exhibit time-temperature superposition for all thicknesses studied, they do not superimpose if different thicknesses are compared. This is illustrated in

Fig. 12. The figure shows $\phi_q^{\rm s}$ versus t/τ_q for $D=5, 20$ and the bulk at comparable distances to the corresponding critical temperature (i.e., $T - T_{\rm c} \simeq 0.045$). Obviously, the shape of the late-time relaxation depends on D. Note that, compared to $\beta_q^{\rm K}(D=20)$, the stretching exponent of the *thinner* film, i.e., $\beta_q^{\rm K}(D=5)$ is closer to that of the bulk. A possible explanation could be as follows: Due to the presence of the walls, there is a distribution of the relaxation times along the transversal direction. Regions closer to the wall decay faster and thus exhibit a smaller relaxation time. On the other hand, as the temperature decreases, the influence of the walls is "felt" throughout the film for all thicknesses studied. There is practically no region of (bulk-like) constant relaxation time in the inner part of the film. Now, if we divide a film into layers in which the relaxation time is calculated, the number of layers is smaller in a thin than in a thick film. The simplest assumption then is that the larger number of layers in the thick film leads to a broader distribution of relaxation times. Of course, if D increases further, there will be a region of bulk-like behavior which grows in the middle of the film and starts to dominate properties of the system for very large D. The film thicknesses studied here, however, are far from this limit.

V. DETERMINATION OF $T_{\rm c}(D)$

The analysis of the preceeding section showed that the relaxation of the films is qualitatively compatible with predictions of mode-coupling theory and that it speeds up with increasing confinement. To some extent, the dynamics of the films corresponds to the behavior of the bulk obtained at a higher temperature. This suggests that confinement reduces the characteristic temperatures of the film compared to those of the bulk. In this section, we want to quantify this reduction by determining the critical temperature $T_{\rm c}(D)$ and the Vogel-Fulcher-Tammann temperature $T_0(D)$.

Mode-coupling theory [22–24] predicts that the relaxation times of any correlation function, which couples to density fluctuations, should exhibit the power-law temperature dependence of Eq. (14) if T is close to $T_{\rm c}$. Indeed, the α-relaxation times of the incoherent and coherent scattering functions in the bulk may be described by Eq. (14) in some q-dependent temperature interval [17,49]. Deviations are found both for temperatures too close and to far away from $T_{\rm c}^{\rm bulk}$. These deviations are theoretically expected. Since Eq. (14) is an asymtotic result of the idealized MCT, it can be violated if T is very close to $T_{\rm c}$ due to relaxation channels which are not treated by the idealized theory, and very far from $T_{\rm c}$ where the asymtotic formula is no longer applicable. Similarly, the q-dependence of the temperature interval, where Eq. (14) is valid, has been rationalized by calculating the leading-order corrections to the asymptotic behavior within the framework of idealized MCT [53,54]. Due to our findings in the bulk and due to the results of the previous section we expect to obtain similar results when analyzing the films.

To examine this expectation, we define relaxation times as the time needed by a given mean-square displacement, like g_1, g_3 or g_0 [see Eqs. (5), (6) and (7)], to reach the monomer size

$$g_i(t=\tau) := 1 \text{ (defining equation for } \tau) \ . \tag{15}$$

This is a reasonable choice because the bulk analysis revealed that a monomer, which has moved across its own diameter, contributes to the α-relaxation [48]. Using Eq. (15) we

computed $\tau(g_i = 1)$ as a function of temperature for various film thicknesses, where, in addition to g_0, g_1 and g_3, the MSD of the end monomers,

$$g_4(t) = \frac{3}{2M} \sum_{i=1}^{M} \left\langle [\boldsymbol{r}_{i,\parallel}^{\rm end}(t) - \boldsymbol{r}_{i,\parallel}^{\rm end}]^2 \right\rangle \ , \tag{16}$$

has also been used. The resulting relaxation times were then fitted by Eq. (14) as follows: First, all (three) parameters of Eq. (14) were adjusted. The results for γ obtained from $\tau(g_0=1)$, $\tau(g_1=1)$, $\tau(g_3=1)$ and $\tau(g_4=1)$ agreed well within the error bars. Therefore, we fixed γ at the average value for the given film thickness and repeated the fits to optimize the remaining parameters.

Table I compiles $T_{\rm c}(D)$ and $\gamma_{\rm MSD}(D)$ obtained in this way. Figure 13 shows a representative example of this analysis. The upper panel depicts $\tau^{-1/\gamma}$ versus T for a film of thickness $D=5$. The intersection of the straight lines (MCT-fit results) with the T-axis yields the critical temperature at this film thickness: $T_{\rm c}(D=5) = 0.305 \pm 0.005$. Note that, despite the highly non-linear relationship between the MSD's used to define the various τ's, all fits yield the same $T_{\rm c}$.

To test this analysis the determined critical temperature can be used to linearize the relaxation time by plotting τ versus $T-T_{\rm c}$ on a log-log scale. The lower panel of Fig. 13 shows that the power law (14) is a good approximation close to $T_{\rm c}$. Analogous to the bulk, there are deviations for large $T-T_{\rm c}$, where the asymptotic regime is left. On the other hand, no deviations are observed for small $T-T_{\rm c}$. In the bulk [17,29], they were only found for $T-T_{\rm c} \lesssim 0.02$ and thus for temperatures smaller than those simulated for $D=5$ up to now.

Furthermore, as indicated by the solid line in the lower panel, $\tau(T)$ can also be described by a Vogel-Fulcher-Tammann (VFT) equation, i.e., by

$$\tau(T) \propto \exp\left[\frac{c(D)}{T - T_0(D)}\right] \ , \tag{17}$$

where c is a constant which can depend on film thickness. The possibility of describing the same data by both a power law (MCT) and a VFT-fit has also been observed for the bulk (see Fig. 10 in [16]). We therefore use the VFT-formula as an independent approach to determine the variation of T_0 with film thickness. Table I contains the results. A plot of $T_{\rm c}(D)$ and $T_0(D)$ is shown in Fig. 14. Since we expect $T_0 < T_{\rm g} < T_{\rm c}$, the figure suggests that also the glass transition temperature, $T_{\rm g}$, should be reduced for stronger confinement. Qualitatively, this result parallels those reported for experiments on supported [9] and on freely standing polystyrene films [7,8,55] as well as for MD simulations of a polymer model similar to ours in the case of weak monomer-substrate attraction [14].

The critical temperatures, $T_{\rm c}(D)$, were determined, for instance, from the mean-square displacement of all monomers [see Eq. (15)] and thus from a quantitiy which corresponds to the low-q limit of the incoherent scattering function. Figure 15 shows that the same $T_{\rm c}(D)$ can also be used to linearize the relaxation times τ_q at maximum of the static structure factor. Here, τ_q was defined by $\phi_q^{\rm s}(t=\tau_q) = 0.3$. The upper panel depicts a log-log plot of τ_q versus $T - T_{\rm c}$ for $D = 5, 7, 10, 15, 20$ and for the bulk. It illustrates that a shift of the temperature scale by $T_{\rm c}(D)$ leads to a very good superposition of the film data for all T studied and also of the film and the bulk if $T-T_{\rm c} > 0.1$. For smaller $T-T_{\rm c}$ deviations occur.

The relaxation time of the bulk increases less steeply than that of the films. This implies that the exponent γ_ϕ of Eq. (14) is smaller in the bulk than in the films. If one fits Eq. (14) to that T-interval, where the film data are linear, one obtains γ_ϕ-values which range between $\gamma_\phi(D=10)=2.68$ and $\gamma_\phi(D=5)=3.24$ and which do not increase monotonically with decreasing D [see table I]. The lower panel of Fig. 15 illustrates the same data in a slightly different way. Here, τ_q^{-1/γ_ϕ} is depicted versus $T-T_\mathrm{c}(D)$. The exponents, γ_ϕ, used for this plot are obtained from fits to Eq. (14) using τ_q as input data and keeping $T_\mathrm{c}(D)$ constant. As expected, curves at all film thicknesses converge towards the origin of coordinates. In other words, the computed critical temperatures are consistent with a temperature dependence of τ_q according to Eq. (14). On the other hand, the curves splay out at large $T-T_\mathrm{c}(D)$ indicating that the prefactor, B, in $\tau_q^{-1/\gamma_\phi}=B\,|T-T_\mathrm{c}(D)|$ depends on the film thickness, D.

As mentioned above, although not monotonically, the exponent γ_ϕ seems to increase with decreasing D [see also table I]. To some extent, this finding is unexpected, given the variation of the Kohlrausch exponent β_q^K in Fig. 12. For the bulk, mode-coupling theory predicts $\lim_{q\to\infty}\beta_q^\mathrm{K}=b$ [56]. Here, b is the von-Schweidler exponent which is related to γ_ϕ by $\gamma_\phi=1/2a+1/2b$ [22–24]. The exponents a (exponent of the "critical decay") and b are correlated with one another. A decrease or an increase of b entails a decrease or an increase of a. When applying these bulk predictions to the films the D-dependence of β_q^K in Fig. 12 [$\beta_q^\mathrm{K}(D=20)<\beta_q^\mathrm{K}(D=5)<\beta_q^{\mathrm{K\,bulk}}$] suggests $b(D=20)<b(D=5)<b_\mathrm{bulk}$ and thus $\gamma_\phi(D=20)>\gamma_\phi(D=5)>\gamma_{\phi,\,\mathrm{bulk}}$. While $\gamma_\phi(D)>\gamma_{\phi,\,\mathrm{bulk}}$ for all D, the results of table I do not confirm the expected order between the different film thicknesses.

However, one should not conclude from the preceding discussion that a consistent application of MCT might not be possible. On the one hand, it is not clear whether the D-dependence of the finite-q result in Fig. 12 (β_q^K at $q=6.9$) is the same as in the limit $q\to\infty$ (i.e., as for b). The corrections to the asymptotic behavior could depend on both q and D. On the other hand, the fitted value for γ_ϕ at $D=5$ is the least certain because the lowest temperature simulated corresponds to a rather large $T-T_\mathrm{c}(D=5)\simeq 0.045$ contrary to $T-T_\mathrm{c}\simeq 0.025$ for $D=20$. Therefore, the simulations have to be extended to lower temperature to test whether there are clear deviations from the superposition of τ_q at low T in Fig. 15. The present quality of the fits would rather suggest that the γ_ϕ-values for the different film thicknesses are very close to each other.

Within the framework of MCT, quantities, such as the exponents a, b or γ and the critical temperature, are determined by the thermodynamic properties of the glass former, in particular by the static structure factor [22–24]. The discussion of Fig. 6 already suggested that $S(q)$ changes with decreasing D in a quite similar fashion as the bulk $S(q)$ if the temperature is increased. Therefore, the question arises of whether it is possible to superimpose the bulk and film results for $S(q)$ by comparing the data for the same $T-T_\mathrm{c}(D)$. This would imply that the reduction of T_c in the films is closely related to the fact that the development of the local packing, characteristic of the supercooled bulk, is shifted to lower temperature by the presence of the smooth walls. Figure 16 shows that such as superpostions for the same $T-T_\mathrm{c}(D)$ is possible if the confinement is not too strong (here, for $D\geq 10$). The upper panel compares $S(q)$ of the bulk with that of a film of thickness $D=10$ for $T-T_\mathrm{c}=0.01$. With the exception of the (slightly) different amplitude of the first maximum, both structure factors are identical over the whole q-range. The lower panel shows the same comparison for the bulk and films of thicknesses $D=5, 10$ and 20 at a larger distance from T_c, i.e., for

$T - T_c = 0.05$. While $S(q)$ of the bulk and film still coincide for $D \geq 10$, this is no longer the case for the thinnest film studied ($D = 5$). The influence of the confinement on the packing structure of the system at this film thickness cannot be explained by a mere shift of the temperature axis.

VI. SUMMARY

Results of extensive MD simulations of thin (non-entangled) polymer films are presented, which focus on the influence of confinement on the sluggish dynamics of the system and in particular on the glass transition temperature. The film geometry is realized by introducing two perfectly smooth and purely repulsive walls. All simulations are carried out at constant normal pressure $P_{N,ext} = 1$.

The static properties of the system show that chains close to the walls prefer a parallel alignment. However, when averaged over the whole film and all directions, the influence of the walls on the chain conformations becomes very weak. In particular, we find that the chains' radius of gyration, R_g^2, does not depend much on film thickness. Even for the extreme case of $D = 5$, R_g^2 lies only by 10% below the corresponding bulk value.

On the level of the overall packing structure of the melt, we observe that the structure factor, $S(q)$, of a film of thickness D resembles that of the bulk at a higher temperature. If the confinement is not too strong ($D \geq 10$), $S(q)$, measured for a particular D at some T', almost coincides with the bulk result for that temperature T'' which lies at the same distance to T_c^{bulk} as T' to $T_c(D)$ [i.e. $T'' - T_c^{bulk} = T' - T_c(D)$]. This indicates that $T - T_c(D)$ is a relevant parameter for our confined system.

This static property of our model finds a counterpart in the dynamic behavior. Our main findings for the dynamics can be summarized as follows: (1) The relaxation of the supercooled films is accelerated compared to the bulk so that characteristic temperatures, such as the mode-coupling critical temperature, $T_c(D)$, or the Vogel-Fulcher-Tammann temperature, $T_0(D)$, decrease with decreasing film thickness. As we expect $T_0 \leq T_g \leq T_c$, our results suggest that also $T_g(D)$ should decrease with decreasing film thickness. (2) The films exhibit several features predicted by mode-coupling theory, such as the space-time factorization property in the intermediate time window of the β-process, time-temperature superposition of the α-relaxation, and a power-law increase of the α-relaxation time in a T-interval that is close, but not too close to T_c. This implies that the implications of the cage effect, whose approximate mathematical treatment leads to these predictions, also seems to be an important factor to understand the dynamics of the confined system in the supercooled state above T_c. (3) A comparison of the mean-square displacements in direction parallel and perpendicular to the walls shows that not only the parallel motion, but also the perpendicular motion is accelerated compared to the bulk if the displacement is sufficiently smaller than the film thickness. However, for a given thickness, the parallel motion is always faster than that in transverse direction. In other words, the enhancement of the dynamics in more pronounced when relaxation processes parallel to the walls are considered. Due to the film geometry, it is clear that the long-time limit of the perpendicular mean-square displacements must be finite. We gave an expression which allows a computation of this limitting value from the density profile of the particle that corresponds to the MSD under consideration (i.e., inner monomer, center of mass, etc.).

ACKNOWLEDGEMENT

We thank J. Horbach for helpful discussions on various aspects of this work. We gratefully acknowledge the financial support by the "Deutsche Forschungsgemeinschaft" (DFG) under the project number SFB262 and by BMBF under the project number 03N6015. We are also indebted to the European Science Foundation for financial support by the ESF Programme on "Experimental and Theoretical Investigations of Complex Polymer Structures" (SUPERNET). Generous grants of simulation time by the computer center at the university of Mainz (ZDV), the NIC in Jülich and the RHRK in Kaiserslautern are also acknowledged.

REFERENCES

[1] X. Zhang and J. Bell, Polymer Engineering and Science **39**, 119 (1999).
[2] J. Rayss, W. Podkoscielny, and J. Widomski, J. Appl. Pol. Sci. **49**, 835 (1993).
[3] R. Armstrong and D. Wright, Electrochimica Acta **38**, 1799 (1993).
[4] F. Garbassi, M. Morra, and E. Ochiello, *Polymer Surfaces: From Physics to Technology* (John Wiley & Sons, New York, 1998).
[5] S. Lätsch, H. Hiraoka, and J. Bargon, in *Polymer/Inorganic Interfaces II*, edited by L. Drzal, R. Opila, N. Peppas, and C. Schutte (Material Research Society, Pittsburgh, 1995), Vol. 385, p. 239.
[6] G. Adam and J. Gibbs, J. Chem. Phys. **43**, 139 (1965).
[7] J. Forrest and J. Mattsson, Phys. Rev. E **61**, R53 (2000).
[8] J. Forrest, K. Dalnoki-Veress, J. Stevens, and J. Dutcher, Phys. Rev. Lett. **77**, 2002 (1996).
[9] J. Keddie, R. L. Jones, and R. Cory, Europhys. Lett. **27**, 59 (1994).
[10] J. L. Keddie, R. A. L. Jones, and R. A. Cory, Faraday Discuss. **98**, 219 (1994).
[11] J. Forrest, K. Dalnoki-Veress, J. Stevens, and J. Dutcher, Phys. Rev. Lett. **77**, 4108 (1996).
[12] J. Forrest and R. Jones, in *Polymer Surfaces, Interfaces and Thin Films*, edited by A. Karim and S. Kumar (World Scientific, Singapore, 2000), pp. 251–294.
[13] J. Forrest, K. Dalnoki-Veress, and J. Dutcher, Phys. Rev. E **56**, 5705 (1997).
[14] J. Torres, P. Nealey, and J. de Pablo, Phys. Rev. Lett. **85**, 3221 (2000).
[15] P. de Gennes, Eur. Phys. J. E **2**, 201 (2000).
[16] C. Bennemann, W. Paul, K. Binder, and B. Dünweg, Phys. Rev. E **57**, 843 (1998).
[17] C. Bennemann, J. Baschnagel, and W. Paul, Eur. Phys. J B **10**, 323 (1999).
[18] M. H. Cohen and D. Turnbull, J. Chem. Phys. **31**, 1164 (1959).
[19] M. H. Cohen and D. Turnbull, J. Chem. Phys. **34**, 120 (1961).
[20] M. H. Cohen and D. Turnbull, J. Chem. Phys. **52**, 3038 (1970).
[21] M. Cohen and G. Grest, Phys. Rev. B **20**, 1077 (1979).
[22] W. Götze, in *Les Houches 1989, Session LI*, edited by J. Hansen, D. Levesque, and J. Zinn-Justin (North-Holland, Amsterdam, 1989), pp. 287–503.
[23] W. Götze and L. Sjögren, Transport Theory and Statistical Physics **24**, 801 (1995).
[24] W. Götze and L. Sjögren, Rep. Prog. Phys. **55**, 241 (1992).
[25] W. Götze, J. Phys.: Condens. Matter **11**, A1 (1999).
[26] W. Götze and T. Voigtmann, Phys. Rev. E **61**, 4133 (2000).
[27] W. Kob, J. Phys.: Condens. Matter **11**, R85 (1999).
[28] C. Bennemann, W. Paul, J. Baschnagel, and K. Binder, J. Phys.: Condens. Matter **11**, 2179 (1999).
[29] C. Bennemann, J. Baschnagel, W. Paul, and K. Binder, Comp. Theo. Poly. Sci. **9**, 217 (1999).
[30] M. Aichele and J. Baschnagel, Eur. Phys. J. E **5**, 229 (2001).
[31] M. Aichele and J. Baschnagel, Eur. Phys. J. E **5**, 245 (2001).
[32] K. Kremer and G. Grest, J. Chem. Phys. **92**, 5057 (1990).
[33] F. Varnik, J. Baschnagel, and K. Binder, J. Phys. IV **10**, 239 (2000).
[34] F. Varnik, J. Baschnagel, and K. Binder, J. Chem. Phys. **113**, 4444 (2000).
[35] H. Meyer and F. Müller-Plate, J. Chem. Phys. (to be published).

[36] F. Varnik, J. Baschnagel, and K. Binder, An Iterative Method for MD or MC Simulations of Planar Systems at Constant Normal Pressure and Constant Plate Separation, preprint.
[37] S. Nosé, J. Chem. Phys. **81**, 511 (1984).
[38] W. Hoover, Phys. Rev. A **31**, 1695 (1985).
[39] S. Nosé and M. Klein, Mol. Phys. **50**, 1055 (1983).
[40] W. Hoover, A. Ladd, and B. Moran, Phys. Rev. Lett. **48**, 1818 (1982).
[41] W. Hoover, Phys. Rev. A **34**, 2499 (1986).
[42] S. Nosé, Mol. Phys. **52**, 255 (1984).
[43] F. Varnik and J. Baschnagel, and K. Binder, Reduction of the Glass Transition Temperature in Polymer Films: A Molecular-Dynamics Study, submitted to Phys. Rev. E (2001).
[44] F. Varnik, Ph.D. thesis, University of Mainz, 2000, available from http://ArchiMeD.uni-mainz.de/pub/2001/0007/.
[45] J. Baschnagel, K. Binder, and A. Milchev, in *Polymer Surfaces, Interfaces and Thin Films*, edited by A. Karim and S. Kumar (World Scientific, Singapore, 2000), pp. 1–49.
[46] I. A. Bitsanis and G. Hadziioannou, J. Chem. Phys. **92**, 3827 (1990).
[47] J.-S. Wang and K. Binder, J. Phys. I France **1**, 1583 (1991).
[48] M. Aichele and J. Baschnagel, Eur. Phys. J. E **5**, 229 (2001).
[49] M. Aichele and J. Baschnagel, Eur. Phys. J. E **5**, 245 (2001).
[50] P. Rouse, J. Chem. Phys. **21**, 1272 (1953).
[51] W. Kob, J. Horbach, and K. Binder, in *Slow dynamics in complex systems*, edited by M. Tokuyama and I. Oppenheim (AIP Press, Woodbury, ADDRESS, 1999), pp. 441–451.
[52] T. Gleim and W. Kob, Eur. Phys. J. **B 13**, 83 (2000).
[53] T. Franosch *et al.*, Phys. Rev. E **55**, 7153 (1997).
[54] M. Fuchs, W. Götze, and M. Mayr, Phys. Rev. E **58**, 3384 (1998).
[55] K. Dalnoki-Veress, C. Murray, C. Gigault, and J. Dutcher, Phys. Rev. E **63**, 31801 (2001).
[56] M. Fuchs, J. Non-Cryst. Solids **172-174**, 241 (1994).

TABLES

D	5	7	10	15	20	bulk
T_0	0.204 ± 0.007	0.253 ± 0.013	0.288 ± 0.006	0.297 ± 0.007	0.308 ± 0.004	0.328± 0.008
T_c	0.305 ± 0.006	0.365 ± 0.007	0.390 ± 0.005	0.405 ± 0.008	0.415 ± 0.005	0.450 ± 0.005
$\gamma_{\rm MSD}$	2.5 ± 0.2	2.4 ± 0.2	2.1 ± 0.1	2.2 ± 0.1	2.1 ± 0.1	1.84 ± 0.1
γ_ϕ	3.24± 0.08	3.15 ± 0.1	2.68 ± 0.08	2.76 ± 0.1	2.74 ± 0.1	2.09 ± 0.07

TABLE I. Survey of the VFT-temperature, T_0, the mode-coupling critical temperature, T_c, and the critical exponents, $\gamma_{\rm MSD}$ and γ_ϕ, for different film thicknesses D and for the bulk. T_0 was determined via fits to Eq. (17) both for the film and for the bulk. The critical temperature, $T_c(D)$, was obtained from fits to Eq. (14). In both cases, fits were done for the relaxation time extracted from mean-square displacements [see Eq. (15)]. $T_c^{\rm bulk}$ was known from previous analyses of incoherent and coherent scattering [17,48,49]. The same result for $T_c^{\rm bulk}$ is also obtained by applying Eq. (14) to the bulk-MSD's. The corresponding critical exponent $\gamma_{\rm MSD}$ is listed in the third row of the table. The critical exponent, γ_ϕ (last row), is obtained from fits to Eq. (14), now using the $\alpha-$relaxation times, $\tau_{q=6.9}$, defined by $\phi_q^{\rm s}(t=\tau_q)=0.3$. In this case, $T_c(D)$ was kept fixed and only the prefactor and γ_ϕ were varied.

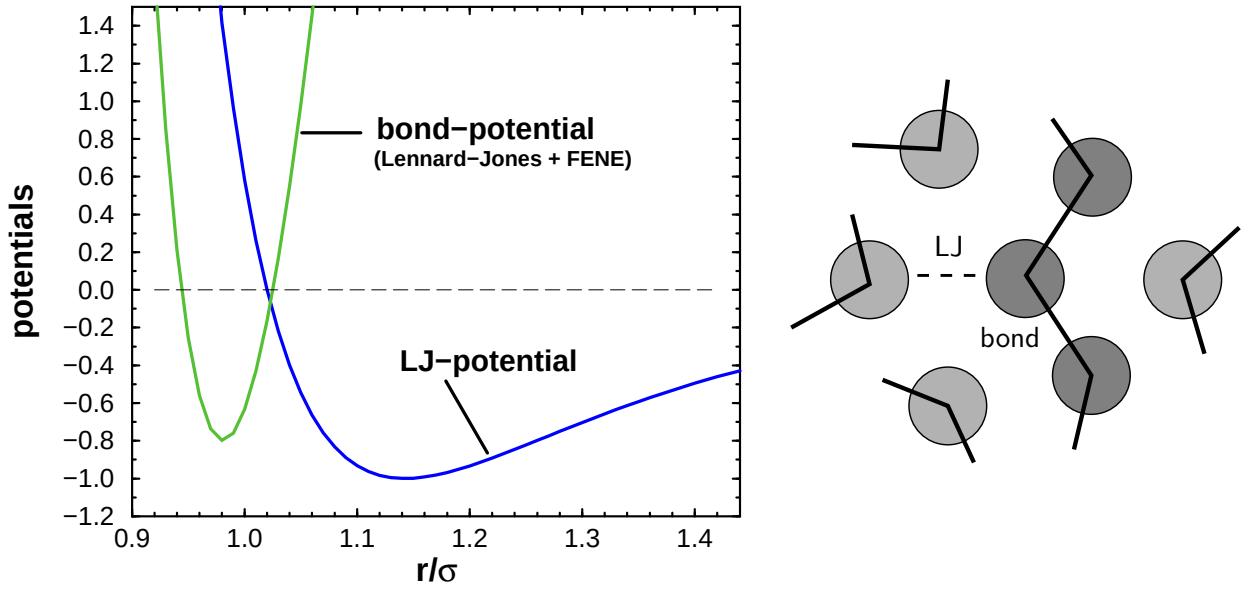

FIG. 1. Left panel: Lennard-Jones potential (LJ) versus the bond potential, the sum of the LJ and FENE potentials. The bond potential is shifted by -20 to lower values for the sake of comparison with the LJ potential. The minimum position of the bond-potential is smaller than that of the LJ-potential: The bond potential has its minimum at $r \simeq 0.96\sigma$, whereas that of a pure LJ-potential lies at $r = \sqrt[6]{2}\sigma$. Due to the incompatibility of these length scales and due to the flexibility of our model (no bond angle or torsion potentials), one expects that cooling the system would not lead to crystallization, but maintain the amorphous structure typical of the liquid phase. This expectation is confirmed by the behavior of static structure factor [see lower panel of Fig. 2]. Right panel: Schematic visualization of the local distortion of the structure due to the two intrinsic length scales of the model.

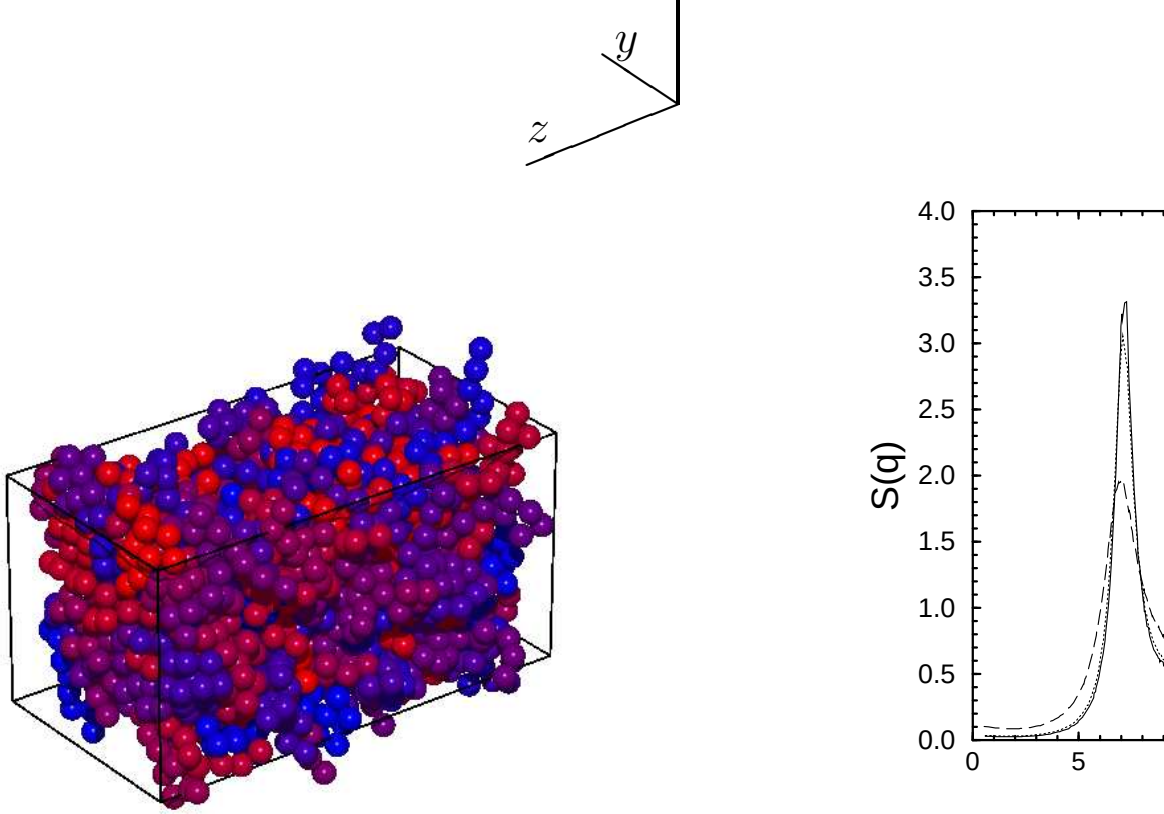

FIG. 2. Upper panel: A snapshot of the simulation box for a film of thickness $D = 20$ at $T = 0.44$. Note that the mode coupling critical temperature of the system at this film thickness is $T_c(D = 20) = 0.415$ (see text and also [43]). A temperature of $T = 0.44$ thus corresponds to the supercooled regime at this film thickness. To visualize the chain structure, a continuous color code is used, monomers of a given chain having the same color. Lower panel: Structure factor $S(q)$ versus the modulus, q, of the wave vector for a film of thickness $D = 10$ at three temperatures: $T = 0.42$, 0.5, and $T = 1$ (the critical temperature of mode-coupling theory for this film thickness is $T_c(D = 10) \simeq 0.39 \pm 0.005$, see Table I). At low temperatures, the peak of the structure factor is more pronounced and its position is slightly shifted towards larger q. This is consistent with the fact that, at lower temperatures, the average interparticle distance decreases. Otherwise, $S(q)$ does not develop sharp peaks for larger q at lower temperatures, thus indicating that the film remains amorphous.

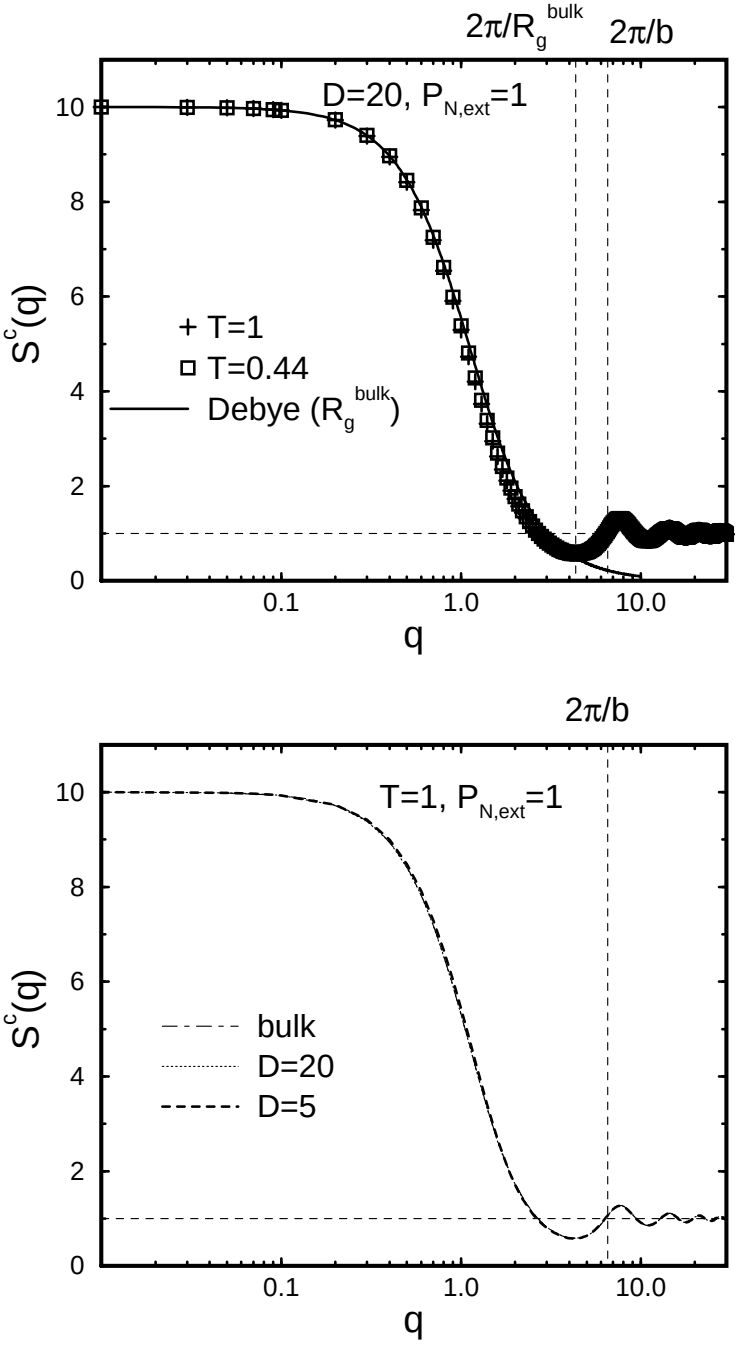

FIG. 3. Upper panel: Chain structure factor, $S^{\rm c}(q)$, for a film of thickness $D=20$ averaged over the whole system. Two representative temperatures are shown: $T=1$ (normal liquid state) and $T=0.44$ (supercooled state) showing that $S^{\rm c}(q)$ is insensitive to a temperature variation. $S^{\rm c}(q)$ in the film is computed in the direction parallel to the walls, i.e. $\boldsymbol{q}=(q_x,q_y)$, $q=|\boldsymbol{q}|$, whereas $\boldsymbol{q}=(q_x,q_y,q_z)$ in the bulk. The solid line indicates the Debye function with $R_{\rm g}^{2\ \rm Debye}=R_{\rm g}^{2\ \rm bulk}$ [see Eq. (3)]. The vertical dashed lines mark the q-values $2\pi/b$ ($b=$ bond length) and $2\pi/R_{\rm g}^{\rm bulk}$. The horizontal dashed line indicates the large q-limit of $S^{\rm c}(q)$. Lower panel: Same as in the upper panel, but now evaluated for the bulk and for films of various thicknesses at $T=1$ (normal liquid state). Apparently, $S^{\rm c}(q)$ is hardly affected by the confinement.

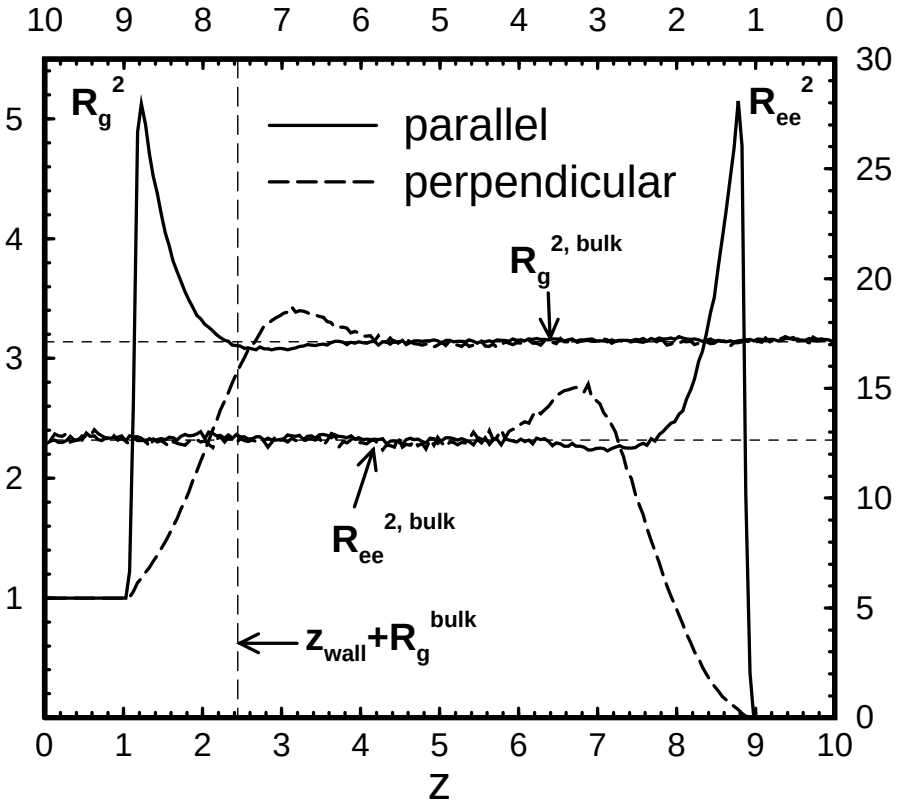
R_g^2
R_{ee}^2
parallel
perpendicular
$R_g^{2,\,bulk}$
$R_{ee}^{2,\,bulk}$
$z_{wall}+R_g^{bulk}$
z

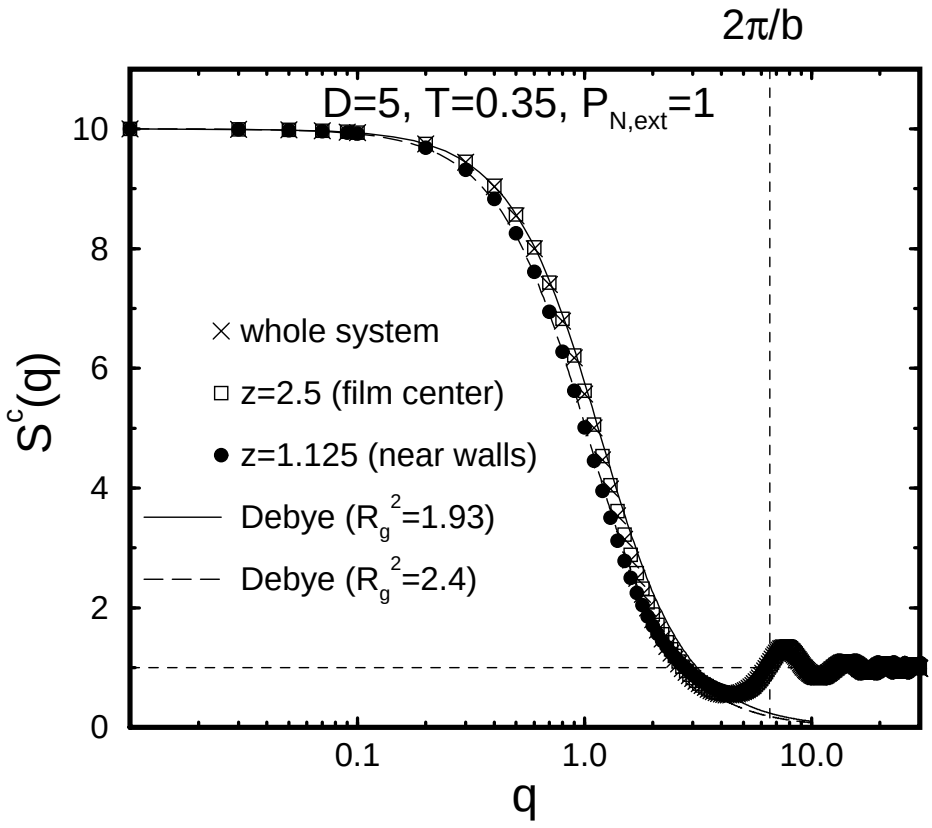
2π/b
D=5, T=0.35, $P_{N,ext}$=1
× whole system
□ z=2.5 (film center)
● z=1.125 (near walls)
Debye (R_g^2=1.93)
Debye (R_g^2=2.4)
$S^c(q)$
q

FIG. 4. Upper panel: Components of the radius of gyration and of the end-to-end distance in directions parallel ($R^2_{g,\parallel}$ and $R^2_{ee,\parallel}$) and perpendicular ($R^2_{g,\perp}$ and $R^2_{ee,\perp}$) to the wall versus the distance, z, from the wall. $R^2_{g,\parallel}(z)$ and $R^2_{ee,\parallel}(z)$ behave qualitatively similar. They develop a maximum close to the wall and then converge towards a constant (bulk) value in the film center (indicated by horizontal dashed lines). Both the bulk radius of gyration and the end-to-end distance are known from previous simulations: $R_g^{2\ \mathrm{bulk}} = 2.14$, and $R_{ee}^{2\ \mathrm{bulk}} = 12.6$ at $T = 1$ and pressure $p = 1$ [16]. The parallel component is multiplied by a factor of 3/2 and the perpendicular one by 3. These factors take into account that compared to three independent directions in the bulk, there are only two independent coordinates in the parallel and one in the perpendicular directions in a planar system. Lower panel: Chain structure factor, $S^c(q)$, evaluated within layers of thickness of 1/4 monomer diameter for a film of thickness $D = 5$ and at the low temperature $T = 0.35$ (supercooled state). Note that the mode-coupling critical temperature for this film thickness is $T_c(D = 5) = 0.305 \pm 0.005$ [see Table I]. A layer close to the wall ($\bullet$) and the layer at the film center ($\square$) are compared to the average of $S^c(q)$ over the whole system ($\times$). The chain structure in the film center coincides with the average behavior of the film. Thus, the deviations of the chain structure in the vicinity of the walls compared to the film center do not crucially influence the average over the whole system. The solid line gives the Debye function with $R_g^{2\ \mathrm{Debye}} = 1.93$, whereas the long dashed line corresponds to $R_g^{2\ \mathrm{Debye}} = 2.4$ [see Eq. (3)]. The values of $R_g^{2\ \mathrm{Debye}}$ are the average radii of gyration calculated over all chains whose center of mass lies in the interval of thickness 1/4 around $z = 1.125$ and $z = 2.375$, respectively. The vertical dashed lines mark the q-values $2\pi/b$ ($b =$ bond length). The horizontal dashed line indicates the large-q behavior of $S^c(q)$ (i.e., $S^c(q \to \infty) = 1$).

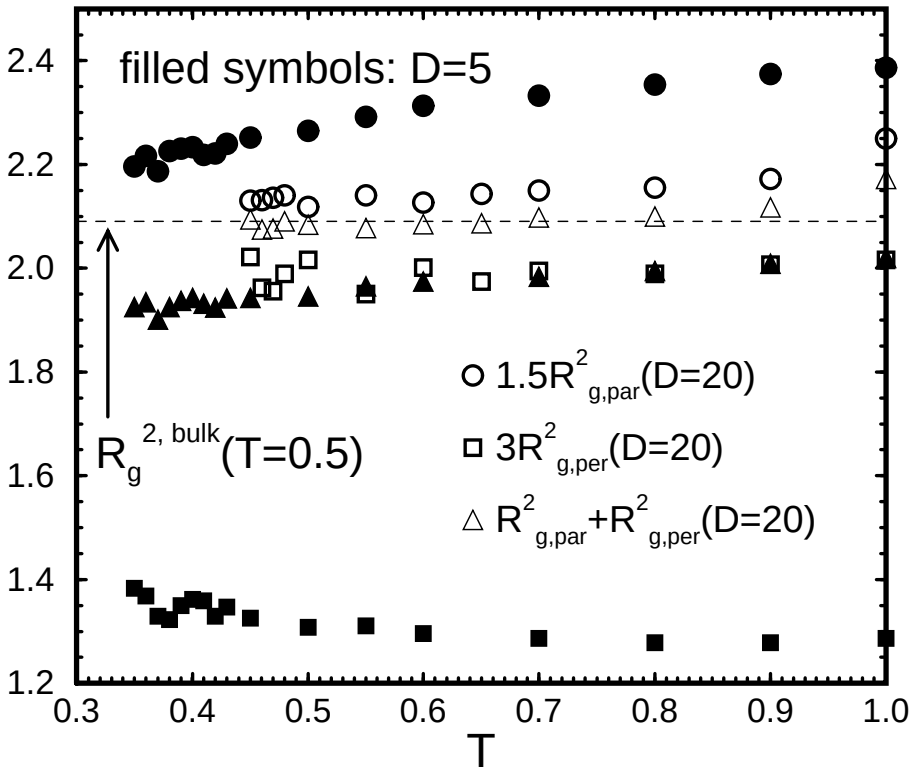
filled symbols: D=5
$1.5R^2_{g,par}(D=20)$
$3R^2_{g,per}(D=20)$
$R^2_{g,par}+R^2_{g,per}(D=20)$
$R_g^{2,\,bulk}(T=0.5)$
2.4
2.2
2.0
1.8
1.6
1.4
1.2
0.3
0.4
0.5
0.6
0.7
0.8
0.9
1.0
T

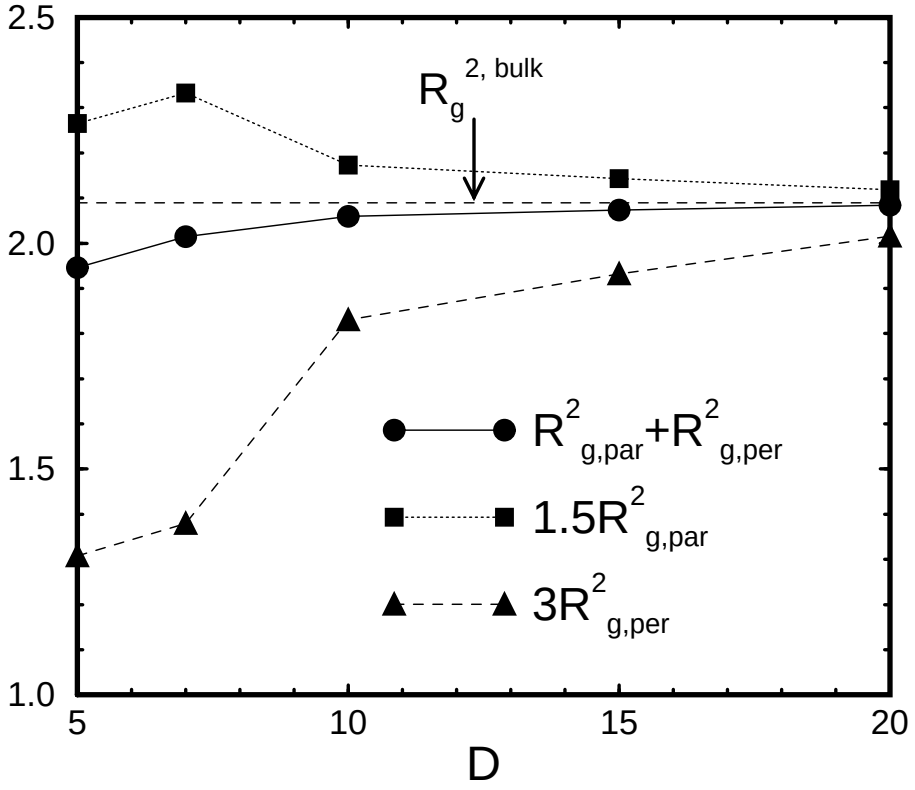
$R_g^{2,\,bulk}$
$R^2_{g,par}+R^2_{g,per}$
$1.5R^2_{g,par}$
$3R^2_{g,per}$
2.5
2.0
1.5
1.0
5
10
15
20
D

FIG. 5. Upper panel: Parallel and perpendicular components of the radius of gyration (1.5 $R^2_{g,\parallel}$ and $3R^2_{g,\perp}$) and their sum, $R^2_g = R^2_{g,\parallel} + R^2_{g,\perp}$, versus temperature. $R^2_{g,\parallel}$ and $R^2_{g,\perp}$ have been computed as (time) averages over all chains in the system. Data are shown for two film thicknesses: $D = 20$ (open symbols) and $D = 5$ (the corresponding filled symbols). The factors 1.5 and 3 are introduced to simplify the comparison with the bulk value. They account for the different number of spatial components in the film for directions parallel (2) and perpendicular (1) to the walls compared to the bulk where there are 3 such components. Both in the case of $D = 20$ and of $D = 5$ chains prefer an alignment parallel to the walls. Due to the opposite changes of $R^2_{g,\parallel}$ and $R^2_{g,\perp}$ with respect to the bulk value, the effect of the confinement on the chain's radius of gyration, $R^2_g = R^2_{g,\parallel} + R^2_{g,\perp}$, is less strong and practically vanishes for $D = 20$. The horizontal dashed line indicates the bulk radius of gyration, $R^{2\ \mathrm{bulk}}_g = 2.09$ (at $T = 0.5$). Lower panel: Same quantities as in the upper panel, now versus film thickness, D, at a temperature of $T = 0.5$. (R^2_g: connected circles, $R^2_{g,\parallel}$: connected squares and $R^2_{g,\perp}$: connected triangles). Again, the parallel orientation is favored by the walls. The overall radius of gyration, however, depends only slightly on film thickness.

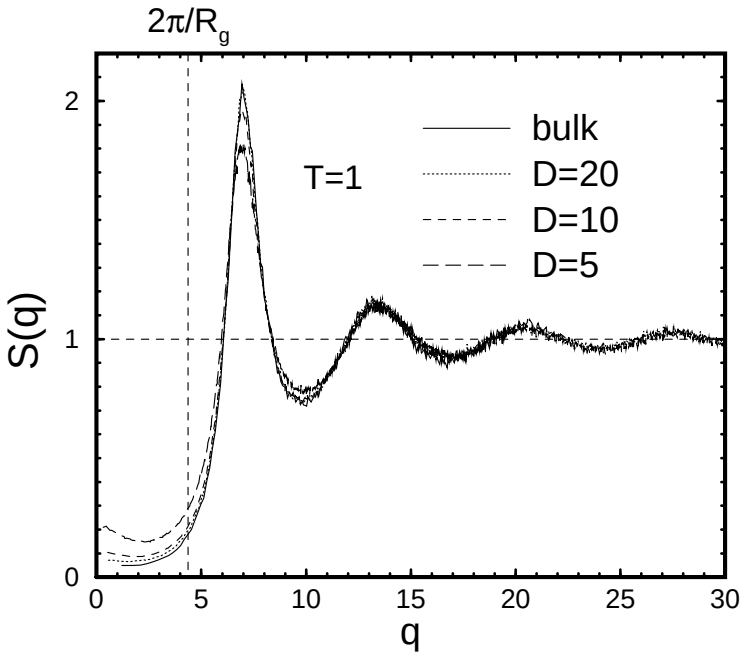
2π/R_g
bulk
D=20
D=10
D=5
T=1
S(q)
q
0
1
2
0
5
10
15
20
25
30

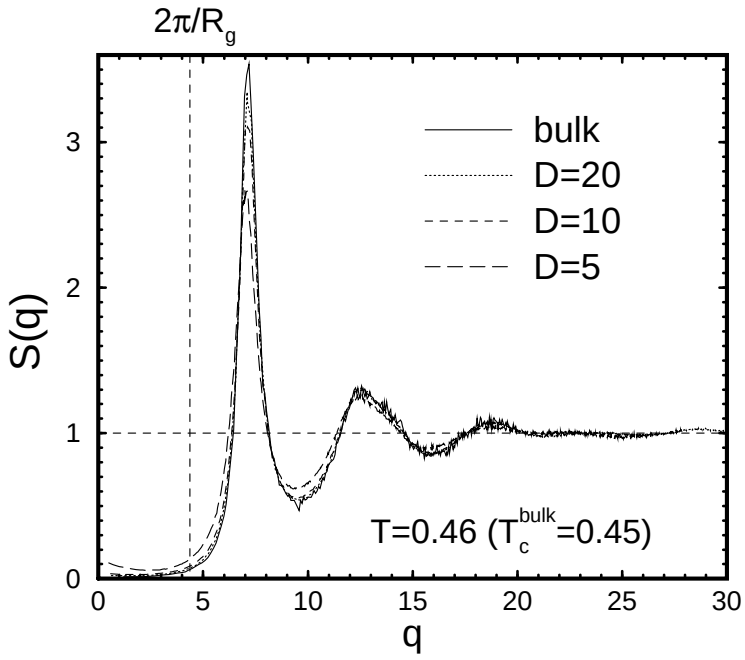
2π/R_g
bulk
D=20
D=10
D=5
T=0.46 (T_c^bulk=0.45)
S(q)
q
0
1
2
3
0
5
10
15
20
25
30

FIG. 6. Upper panel: Structure factor, $S(q)$, of the melt for the bulk and films of various thicknesses ranging from $D = 5\,(\approx 3.5R_{\rm g})$ to $D = 20\,(\approx 14R_{\rm g})$ at a temperature of $T = 1$ (normal liquid state). Note that the mode-coupling critical temperature of the system in the bulk is $T_{\rm c}^{\rm bulk} = 0.45$ [16,17] (see also Table I). $S(q)$ in the film is computed by taking into account the coordinates parallel to the walls only, i.e. $\boldsymbol{q}=(q_x, q_y)$, $q=|\boldsymbol{q}|$. At $T=1$, the structure factor of the thickest film ($D=20$) coincides with that of the bulk. For film thicknesses $D \leq 10$, the influence of the walls on $S(q)$ is visible even at this high temperature. The peak value of $S(q)$ decreases with stronger confinement (smaller D) and the position of the peak is slightly shifted towards smaller q, reflecting an increase of the (average) interparticle distance. Instead of decreasing the film thickness, these changes in $S(q)$ can also be achieved by increasing the temperature only. So, the inverse film thickness plays a qualitatively similar role to that of the temperature. For the largest film thickness shown here, however, the structure factor of the film is identical to that of the bulk over a large q-range. Lower panel: The same as in the upper panel, now for a lower temperature of $T = 0.46$ (supercooled state). Contrary to $T = 1$, the structure factor of the film with $D = 20$ no longer coincides with $S(q)$ of the bulk. Thus, at lower temperatures, the confinement has a stronger impact on the packing structure of the melt.

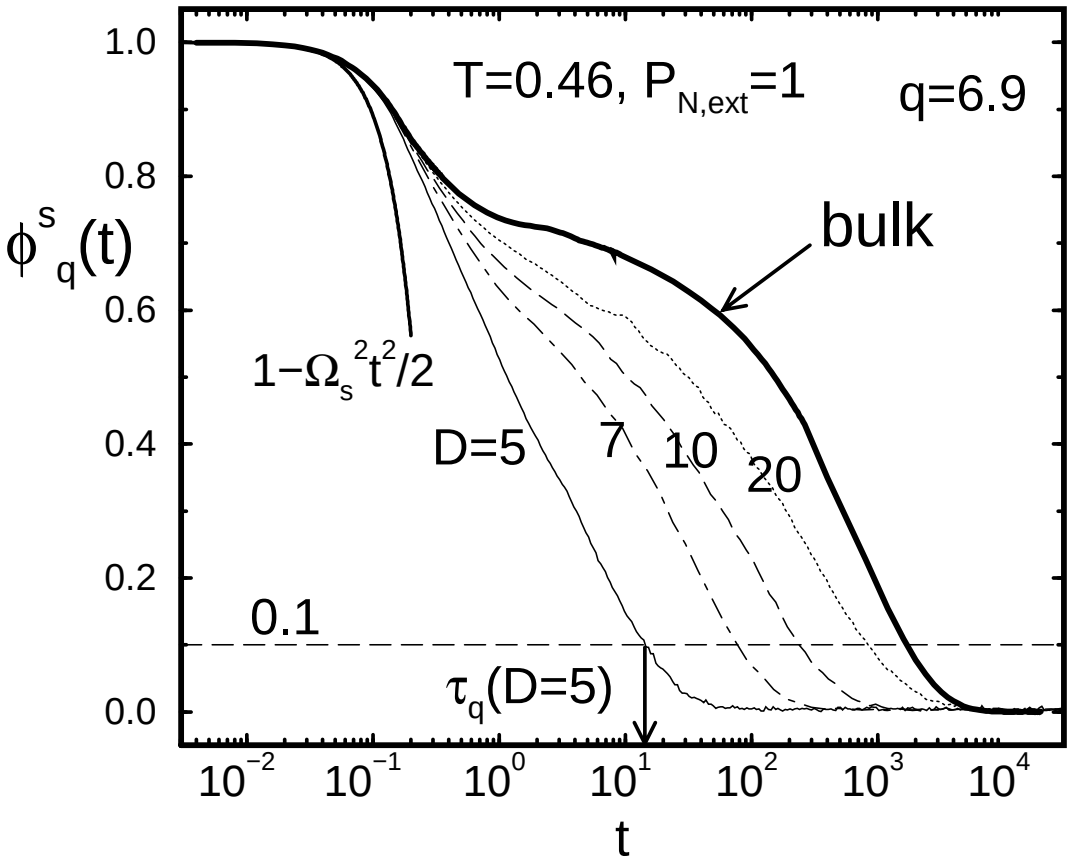

FIG. 7. Comparison of the incoherent intermediate scattering function, $\phi_q^{\rm s}(t)$, at $T = 0.46$ ($T_{\rm c}^{\rm bulk} = 0.45$) for the bulk and films of various thicknesses ranging from $D = 5 \approx 3.5R_{\rm g}$ to $D = 20 \approx 14R_{\rm g}$. $P_{\rm N,ext} = 1$ denotes the pressure of the simulation. The scattering functions are calculated at $q = 6.9$ (maximum of $S(q)$, see Fig. 2). The initial decay of $\phi_q^{\rm s}(t)$ is determined by free ballistic motion, i.e., $\phi_q^{\rm s}(t) = 1 - (\Omega_{\rm s}t)^2/2$ with $\Omega_{\rm s} = q\sqrt{k_{\rm B}T}$. The dashed horizontal line at $\phi_q^{\rm s}(t) = 0.1$ and the vertical arrow on the curve for $D = 5$ indicate how the α-relaxation time, τ_q, is defined. It is the time value when the scattering function has decayed to 0.1.

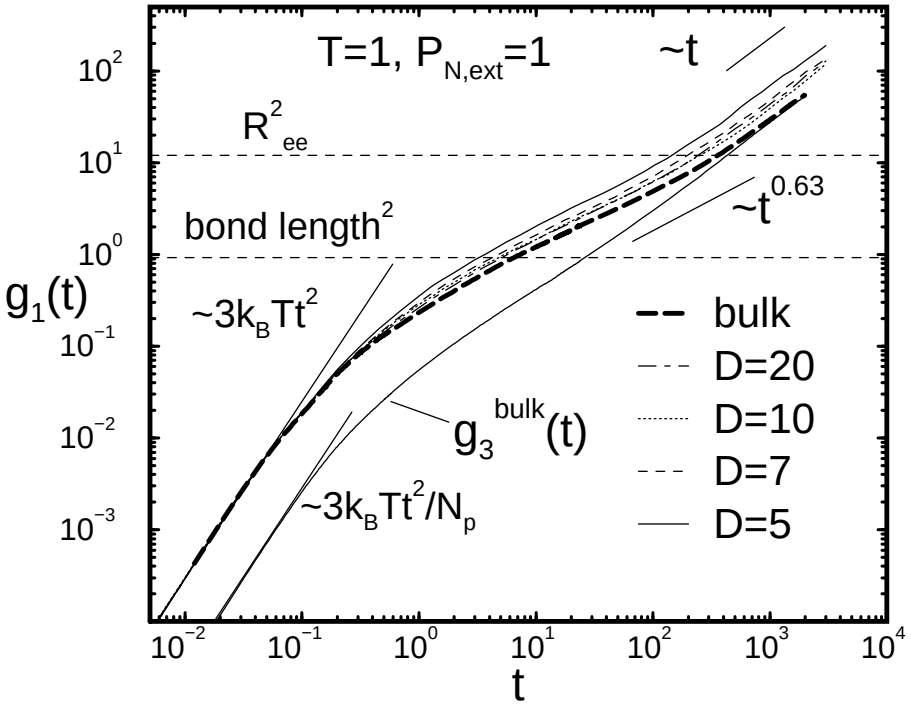
T=1, P_N,ext=1
~t
R^2_ee
bond length^2
~t^0.63
g_1(t)
~3k_BTt^2
bulk
D=20
D=10
D=7
D=5
g_3^bulk(t)
~3k_BTt^2/N_p
t

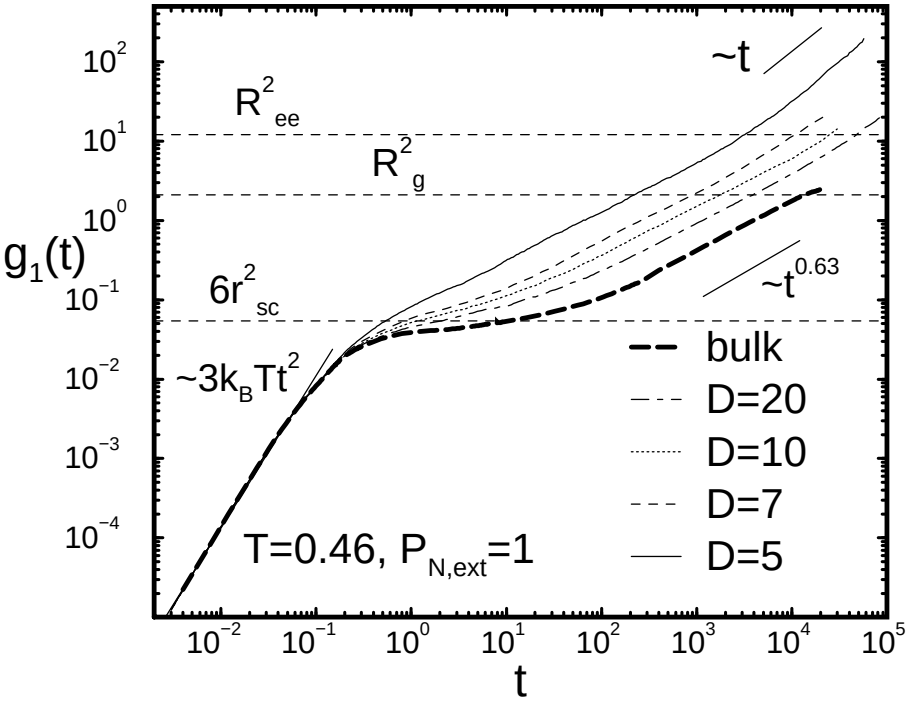
~t
R^2_ee
R^2_g
g_1(t)
6r^2_sc
~t^0.63
~3k_BTt^2
bulk
D=20
D=10
D=7
D=5
T=0.46, P_N,ext=1
t

FIG. 8. Upper panel: Log-log plot of the mean-square displacement of innermost monomers, $g_1(t)$, at $T=1$ (normal liquid state far above $T_c^{\rm bulk}=0.45$). The figure compares the bulk data with the displacements measured parallel to the walls in films of different thicknesses ranging from $D=5$ ($\approx 3.5R_g$) to $D=20$ ($\approx 14R_g$). The film data were multiplied by 3/2 to account for the different number of spatial directions used to calculate $g_1(t)$ (i.e., 3 directions for the bulk, but only 2 for the films). The bulk end-to-end distance R_{ee}^2 ($=12.3$) and the average bond length $b^2=0.922$ are indicated as horizontal dashed horizontal lines. The solid lines represent the behavior of $g_1(t)$ expected in different time regimes: ballistic at short times ($g_1(t) \sim t^2$), diffusive at late times ($g_1(t) \sim t$), and dominated by chain connectivity for times where $g_1(t) > b^2$ ($g_1(t) \sim t^x$; $x=0.63=$ effective exponent in the bulk). For comparison, the MSD of chain's center of mass, $g_3(t)$, is also depicted: At short times, $g_3(t)=3k_BTt^2/N_p$, where $N_p=10$ is the degree of polymerization (number of the monomers of a chain). Contrary to the innermost monomers, the motion of the chain's center of mass is not affected by chain connectivity. Therefore, $g_3(t)$ does not show a $t^{0.63}$-behavior, but continuously crosses over to the diffusive regime which is reached for $g_3(t) \geq R_g^2$ ($=2.14$ at $T=1$). The effects of confinement are rather weak at this high temperature: $g_1(t)$ for $D=10$ and $D=20$ are practically indistinguishable from that of the bulk. For strong confinement ($D=5$ and $D=7$), however, a dependence on film thickness is observed. Lower panel: Same as in the upper panel, now at a low temperature of $T=0.46$ (supercooled state close to $T_c^{\rm bulk}=0.45$). The lowest horizontal line shows the plateau value $6r_{sc}^2$ of a MCT-analysis ($\simeq 0.054$). Again, the solid lines represent the behavior of $g_1(t)$ expected in different time regimes: ballistic at short times ($g_1(t) \sim t^2$), diffusive at late times ($g_1(t) \sim t$), and dominated by chain connectivity for times where $g_1(t) > b^2$ ($g_1(t) \sim t^x$; $x=0.63=$ effective exponent in the bulk). At this low temperatuure, the effect of the walls is much more pronounced compared to $T=1$ (see the upper panel). In both panels $P_{N,ext}=1$ denotes the pressure of the simulation.

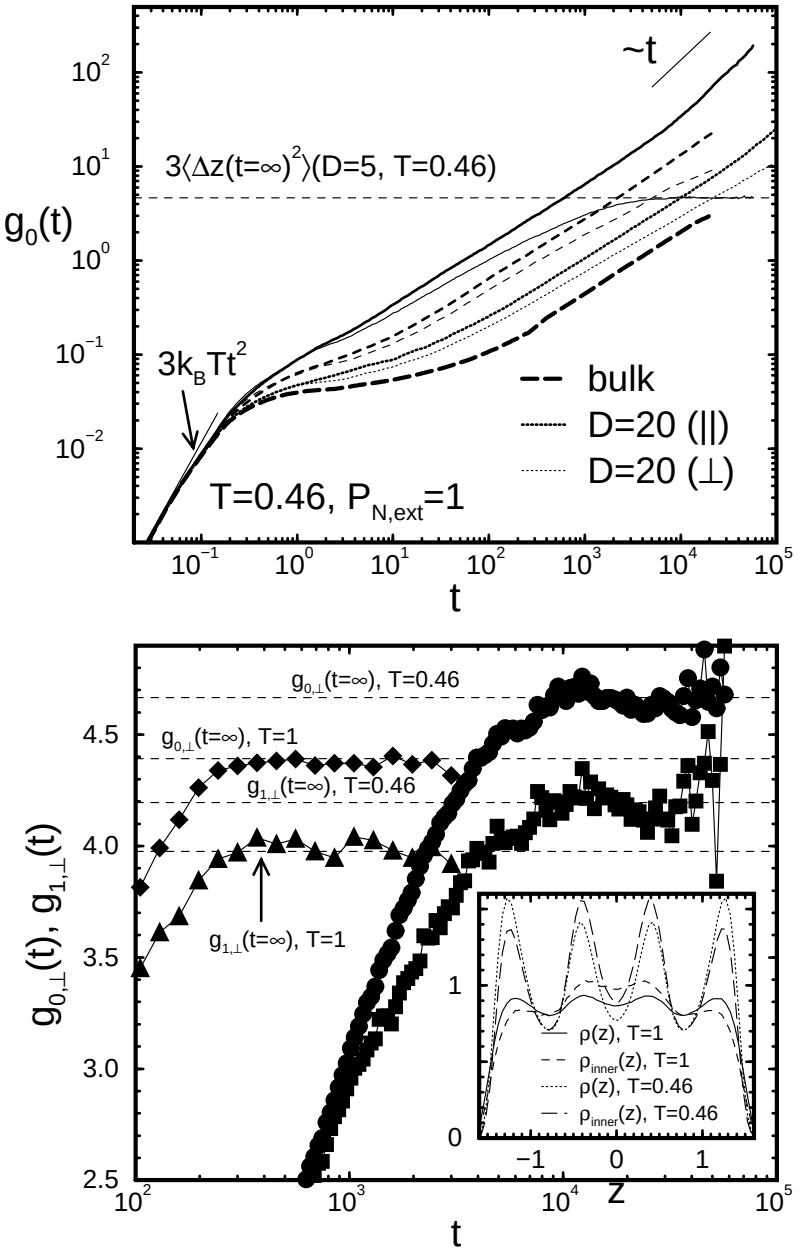
~t
3⟨Δz(t=∞)²⟩(D=5, T=0.46)
g0(t)
3kBTt²
bulk
D=20 (||)
D=20 (⊥)
T=0.46, PN,ext=1
t
g0,⊥(t=∞), T=0.46
g0,⊥(t=∞), T=1
g1,⊥(t=∞), T=0.46
g1,⊥(t=∞), T=1
g0,⊥(t), g1,⊥(t)
ρ(z), T=1
ρinner(z), T=1
ρ(z), T=0.46
ρinner(z), T=0.46
z
t

FIG. 9. Upper panel: Log-log plot of the mean-square displacement of all monomers, $g_0(t)$, at $T=0.46$ (supercooled state). The figure compares the bulk data with the displacements measured parallel ($\|$) and perpendicular ($\perp$) to the walls in films of different thicknesses: $D=5$ ($\|$: thick solid line, $\perp$: thin solid line), $D=7$ ($\|$: thick dashed line, $\perp$: thin dashed line) and $D=20$ ($\|$: thick dotted line, $\perp$: thin dotted line). The film data were multiplied by 3/2 for the parallel direction and by 3 for the perpendicular one to account for the different number of spatial directions used to calculate $g_0(t)$ (i.e., 3 directions for the bulk, 2 for the parallel direction and 1 for the perpendicular direction in the film). The dashed horizontal line indicates the large-t limit of $g_{0,\perp}(t)$ expected from Eq. (9) for a film of thickness $D=5$. Lower panel: Test of Eq. (9) for $g_{0,\perp}(t=\infty)$ and $g_{1,\perp}(t=\infty)$ at $T=1$ and $T=0.46$ [$g_{0,\perp}(t\,;T=0.46)=$ connected circles, $g_{1,\perp}(t\,;T=0.46)=$ connected squares, $g_{0,\perp}(t\,;T=1)=$ connected diamonds and $g_{1,\perp}(t\,;T=1)=$ connected triangles]. The film thickness is again $D=5$. The density profiles of all monomers and of the innermost monomer are depicted in the inset. At the lower temperature of $T=0.46$, both density profiles develop pronounced peaks close to the walls, whereas the density in the film center is rather decreased compared to $T=1$. Larger transversal distances thus contribute more to the MSD in the z-direction. Therefore, we expect an increase of $g_{0,\perp}(t=\infty)$ and $g_{1,\perp}(t=\infty)$ at lower T [see also the text]. As seen in this panel, this expectation is indeed observed in the long time part of $g_{0,\perp}(t)$ and $g_{1,\perp}(t)$, respectively.

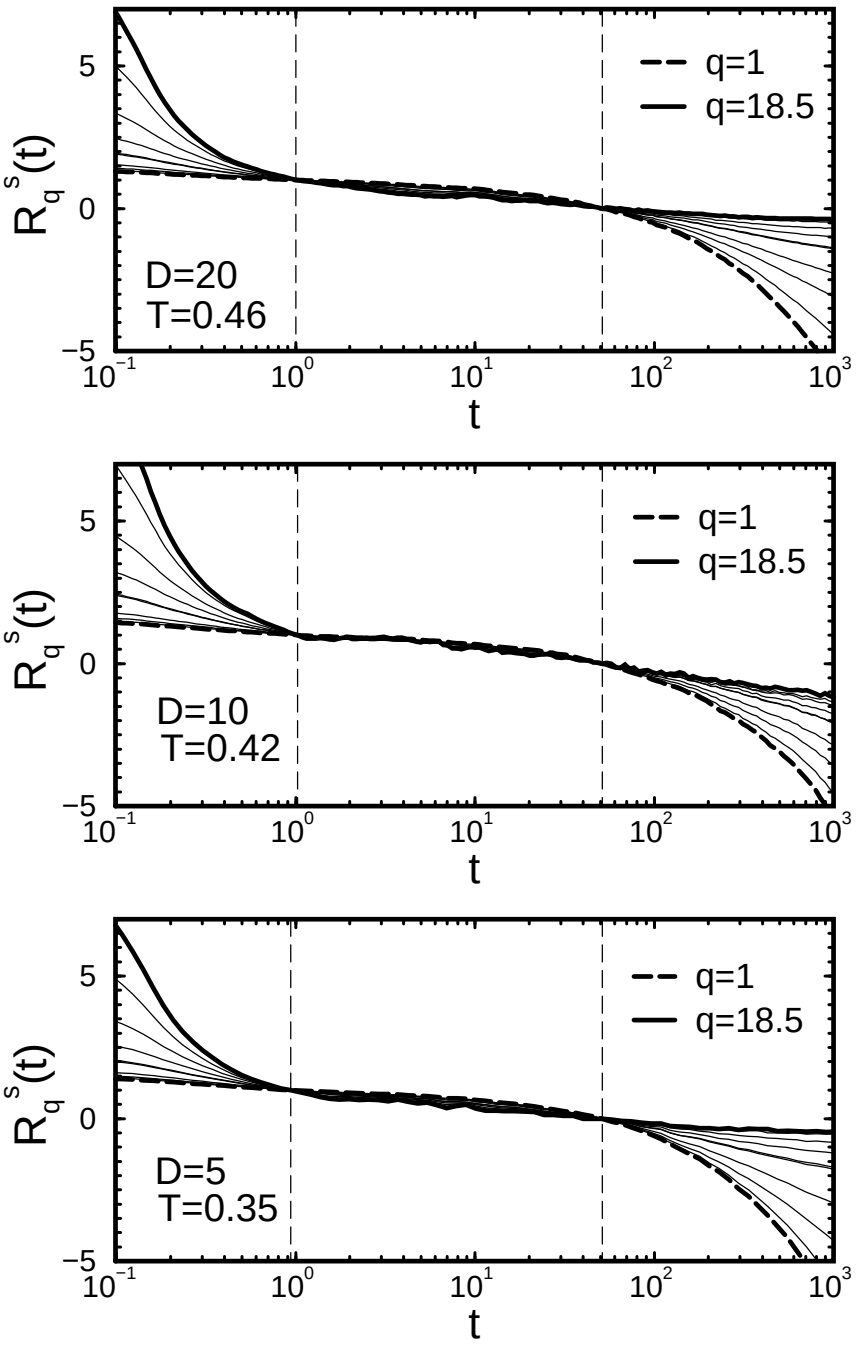

FIG. 10. Test of the space-time factorization theorem [Eq. (10)] for the incoherent intermediate scattering function $\phi_q^{\rm s}(t)$ via the ratio $R_q^{\rm s}(t)$ defined by Eq. (11). The three panels show the results for different film thicknesses and temperatures: $D=20$, $T=0.46$ ($\hat{=}T-T_{\rm c}=0.045$), $D=10$, $T=0.42$ ($\hat{=}T-T_{\rm c}=0.03$), $D=5$, $T=0.35$ ($\hat{=}T-T_{\rm c}=0.045$). The smallest ($q=1$) and the largest ($q=18.5$) wave vectors are highlighted by a thick dashed line and a thick solid line, respectively. The thin solid lines in between refer to the following q-values (from bottom to top): $q=1.8$, 3, 4.3, 6.9, 7.1, 9.5, 12.5, 16. The vertical dashed lines indicate the choices for t'' (left line) and t' (right line). By definition, $R_q^{\rm s}(t'')=1$ and $R_q^{\rm s}(t')=0$.

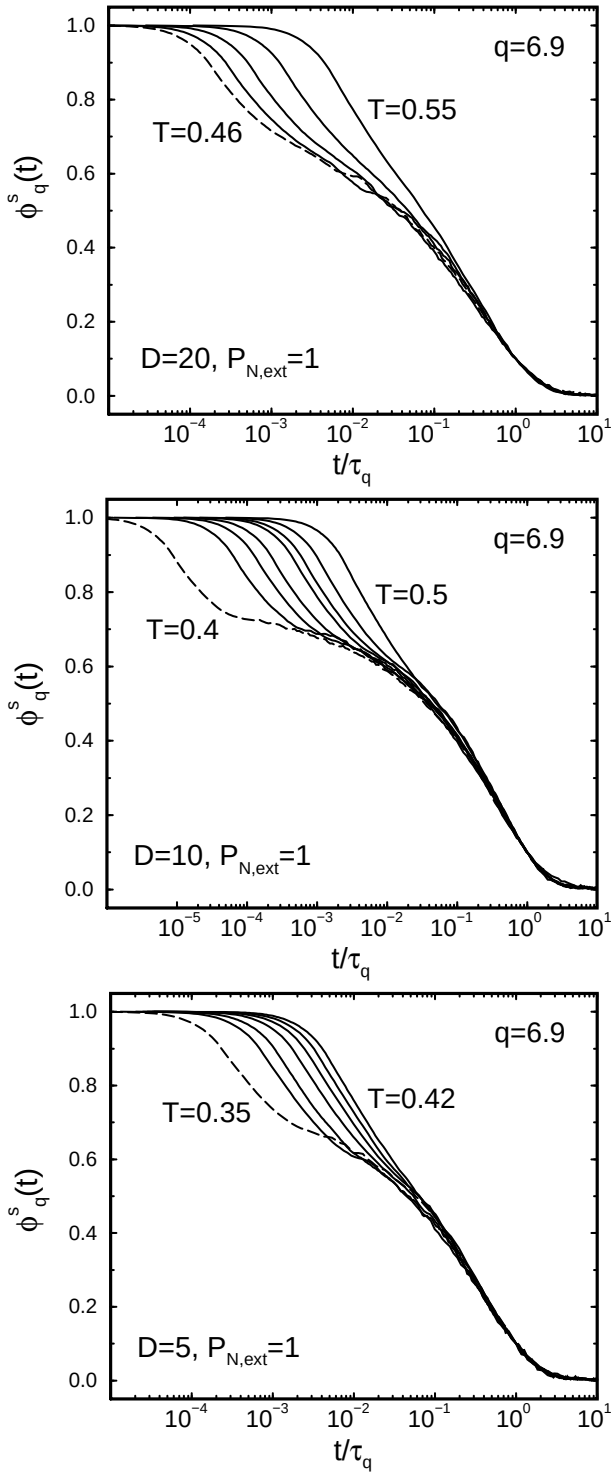

FIG. 11. Test of the time-temperature superposition principle [Eq. (12)] for three different film thicknesses. Top panel: $D = 20$. Temperatures shown are from left to right: $T = 0.46$ ($\hat{=} T - T_c = 0.045$), 0.47, 0.48, 0.48, 0.5, 0.55 . Middle panel: $D = 10$. Temperatures shown are from left to right: $T = 0.4$ ($\hat{=} T - T_c = 0.01$), 0.42, 0.43, 0.44, 0.45, 0.46, 0.47, 0.5. Bottom panel: $D = 5$. Temperatures shown are from left to right: $T = 0.35$ ($\hat{=} T - T_c = 0.045$), 0.37, 0.38, 0.39, 0.4, 0.41, 0.42. In all three panels the time axis is rescaled by the α-relaxation time, τ_q, defined by $\phi_q^s(t = \tau_q) = 0.1$, and the lowest temperature is depicted by a dashed line.

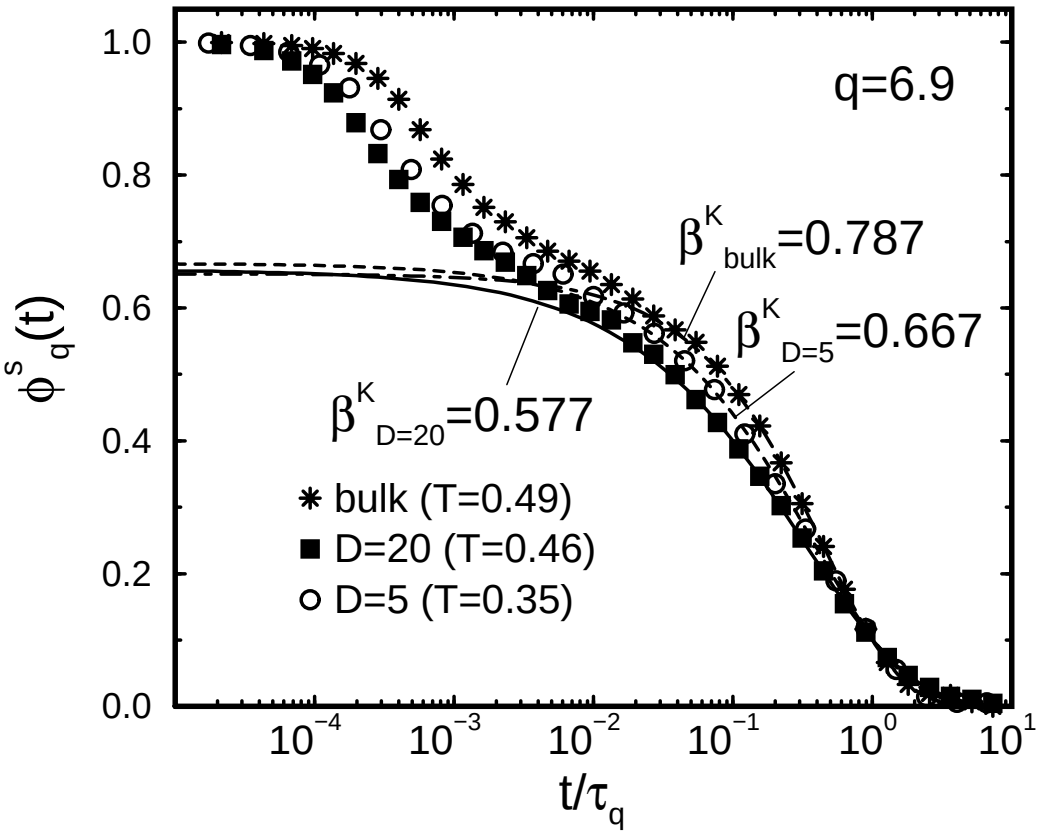

FIG. 12. Incoherent intermediate scattering function $\phi_q^{\rm s}(t)$, calculated at the maximum of $S(q)$ ($q=6.9$), versus rescaled time t/τ_q for $D=5,20$ and the bulk. τ_q is defined by $\phi_q^{\rm s}(t=\tau_q)=0.1$. The temperatures shown roughly correspond to the same distance to $T_{\rm c}$, i.e., to $T-T_{\rm c}\simeq 0.045$, for both the films and the bulk. In addition, the results of KWW-fits [Eq. (13)] to the long-time behavior of $\phi_q^{\rm s}(t)$ are depicted ($D=5$: dashed line, $D=20$: solid line, bulk: dot-dashed line). The corresponding stretching exponents are indicated in the figure. In all three cases, only data with $t/\tau_q>0.05$ were used for the KWW-Fit.

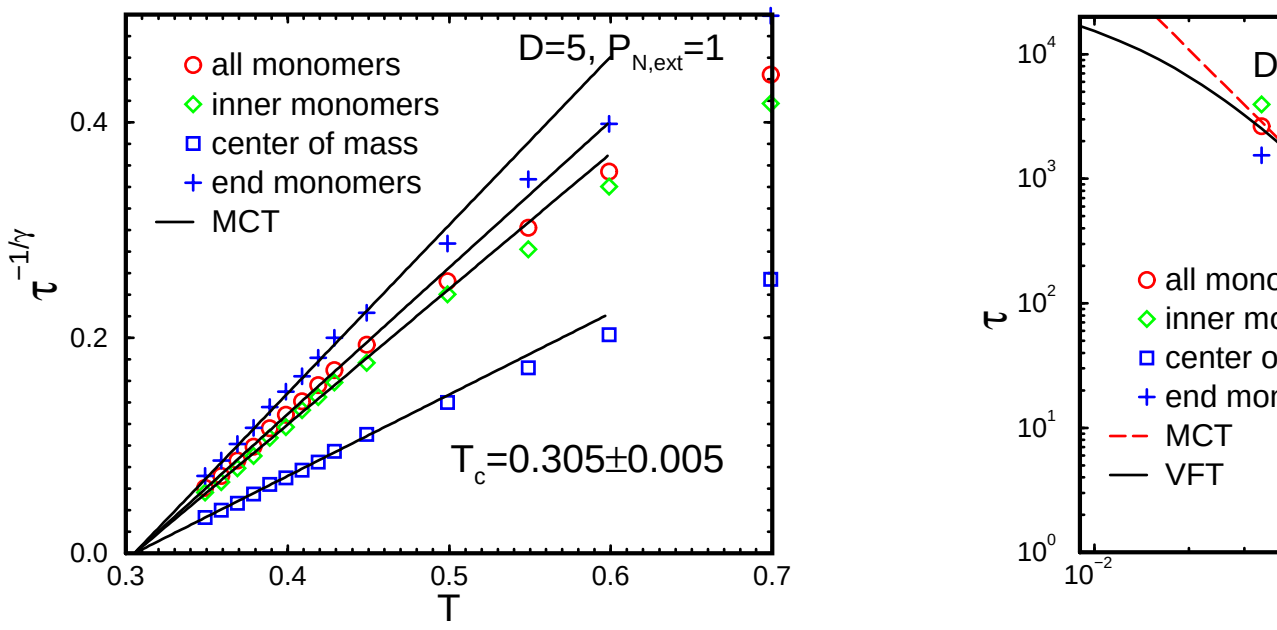

FIG. 13. Upper panel: Plot of $\tau^{-1/\gamma}$ versus T for $D=5$. The relaxation time τ was determined by Eq. (15) using the mean-square displacements (MSD) of inner-, end- and all monomers and of the chain's center of mass. The exponent γ was first determined by fits to Eq. (14) with three open parameters. Since the results for all MSD's agreed within the error bars ($\gamma=2.5\pm0.2$), $\gamma=2.5$ was used in the plot. The fits to Eq. (14) are represented by straight lines. The intersection of these lines with the T-axis determines the critical temperature of the film ($T_c(D=5)=0.305\pm0.005$). Lower panel: Different representation of the same data. Now, τ is plotted versus $T-T_c$ ($T_c(D=5)=0.305$). The dashed line indicates the MCT-fit [Eq. (14)] using $\gamma=2.5$, whereas the solid line represents a fit to the VFT-equation [Eq. (17)] with $T_0(D=5)=0.204\pm0.026$. Both fits shown here were done for $g_1(t)$.

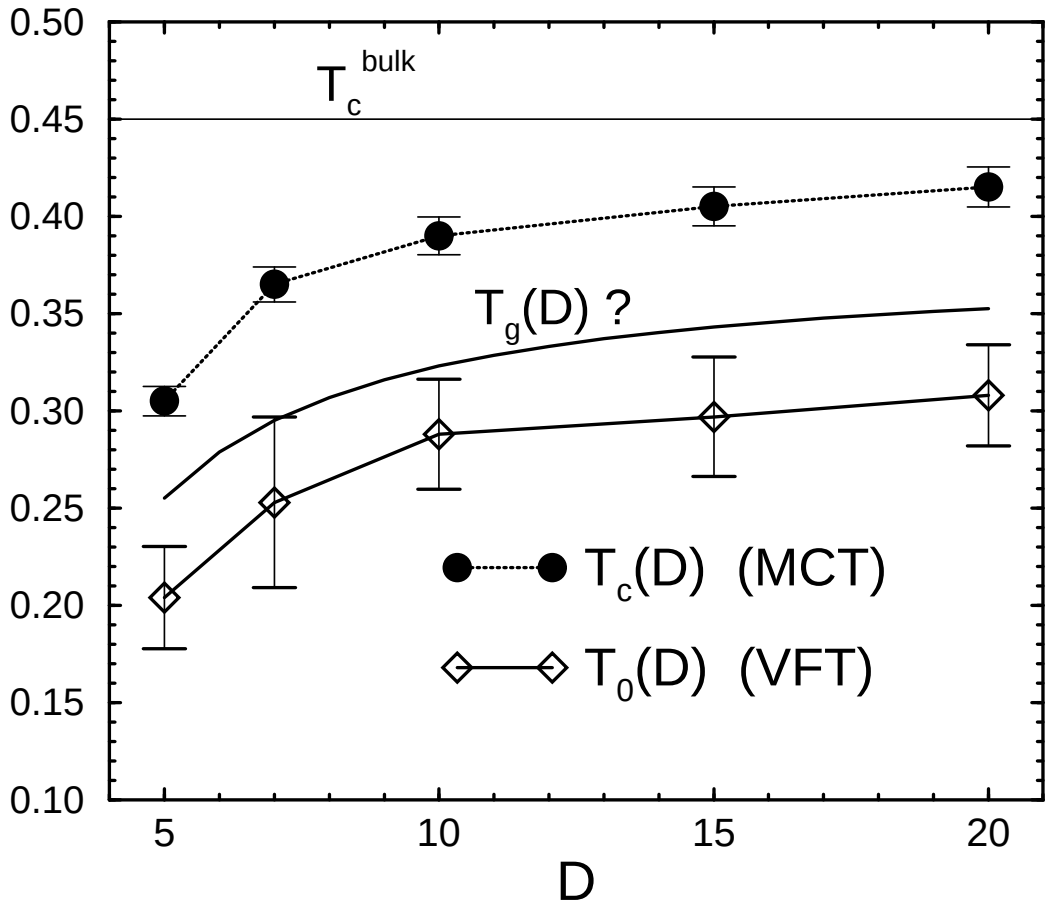

FIG. 14. Mode-coupling critical temperature, $T_{\rm c}(D)$, and the VFT-temperature $T_0(D)$ versus film thickness D. $T_{\rm c}(D)$ was obtained from fits to Eq. (14). Similarly, the VFT-temperatures, $T_0(D)$, and $T_0^{\rm bulk}$ are results of fits to Eq. (17). Note that, the glass transition temperature $T_{\rm g}$ lies *between* these two temperatures: $T_{\rm c} < T_{\rm g} < T_0$. Thus, $T_{\rm g}(D)$ lies somewhere between $T_0(D)$ and $T_{\rm c}(D)$. The solid line gives a suggestion for the possible form of $T_{\rm g}(D)$.

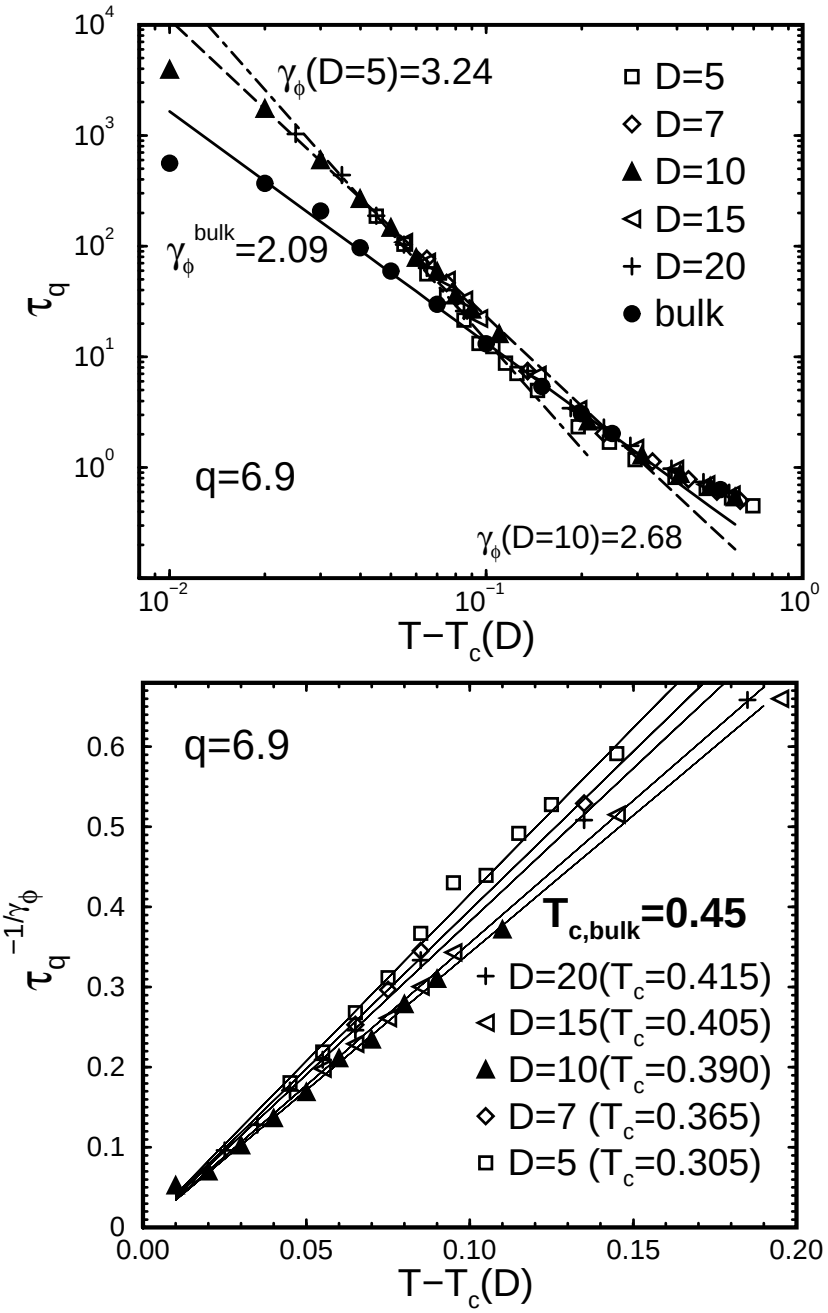

FIG. 15. Upper panel: Relaxation times, τ_q, at the maximum of $S(q)$ ($q=6.9$) versus $T-T_c$ for various film thicknesses ranging from the smallest value studied ($D=5\approx 3.5R_g$) to the largest one ($D=20\approx 14R_g$). τ_q was determined from the incoherent scattering function by requiring $\phi_q^s(t=\tau_q)=0.3$, whereas the critical temperatures, $T_c(D)$, were obtained from the analysis of the mean-square displacements, i.e. from power-law fits to τ by Eq. (14). The lines represent fits of τ_q to Eq. (14) in the regime where the data are linear: $D=5$ (dash-dotted line), $D=10$ (dashed line), bulk (solid line). The resulting values for $\gamma_\phi(D)$ are indicated in the figure. Upper panel: Using the critical exponents, $\gamma_\phi(D)$, obtained from the upper panel of this figure, τ_q^{-1/γ_ϕ} is plotted versus $T-T_c(D)$ for the film data. The lines are again fits to Eq. (14). The deviations from the power law Eq. (14), visible for $D=10$ at $T-T_c(D)=0.01$ in the upper panel, cannot be seen in this representation of the data.

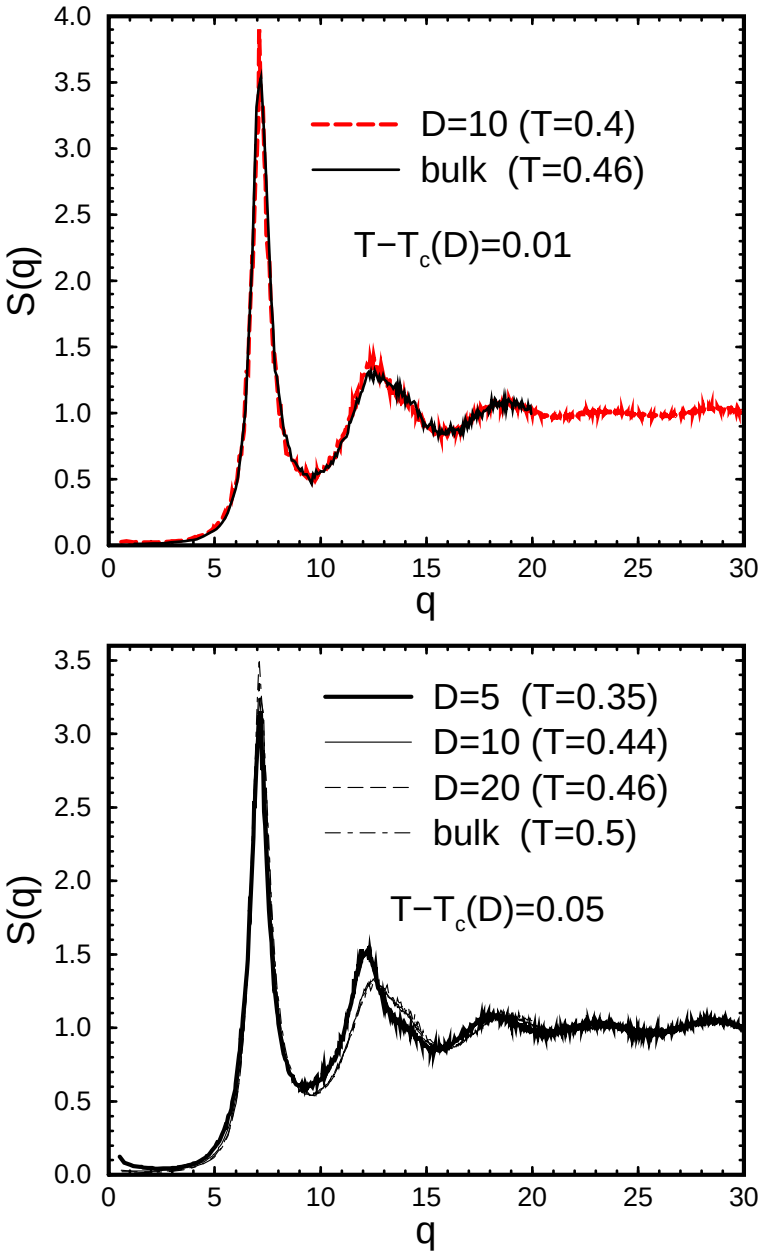

FIG. 16. Upper panel: Collective structure factor, $S(q)$, of the melt for a film of thickness $D = 10$ and for the bulk at temperatures $T = 0.4$ and $T = 0.46$, respectively. Note that $T_c(D = 10) = 0.39$ and $T_c^{\rm bulk} = 0.45$. Thus, the chosen temperatures have the same distance from the corresponding critical temperature, i.e. $0.4 - T_c(D = 10) = 0.46 - T_c^{\rm bulk} = 0.01$. Except the (slightly) different amplitude of the main peak, $S(q)$ of the film and the bulk are essentially identical when compared for the same difference to the critical temperature. Lower panel: Same as in the upper panel for a distance of 0.05 from $T_c(D)$, where data of many film thicknesses are compared to that of the bulk. Again, for film thicknesses $D \geq 10$, $S(q)$ of the film overlaps with that of the bulk. For the extreme case of $D = 5$, however, deviations are not negligible.

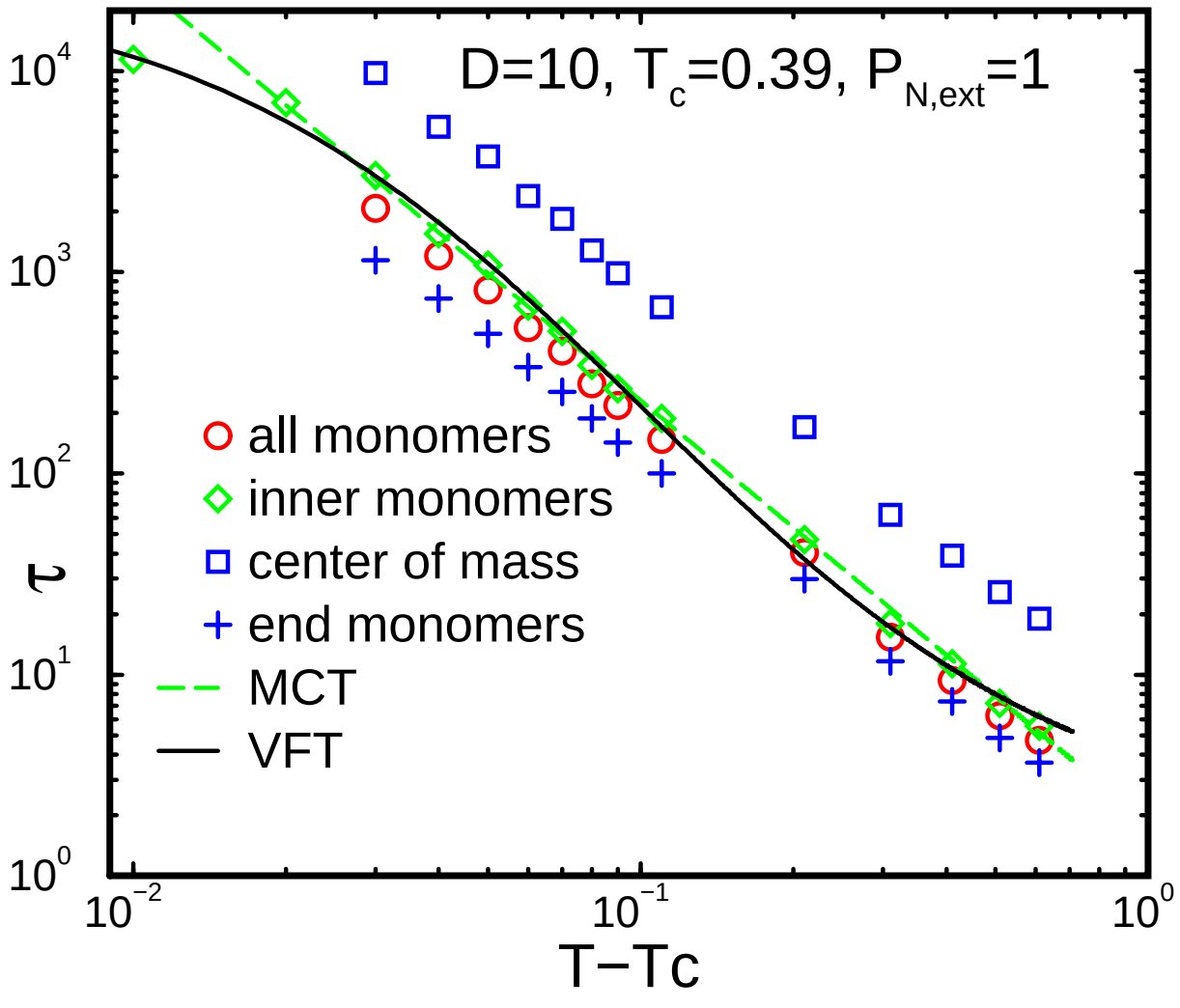
D=10, T_c=0.39, P_N,ext=1
all monomers
inner monomers
center of mass
end monomers
MCT
VFT
τ
T−Tc
10^4
10^3
10^2
10^1
10^0
10^−2
10^−1
10^0

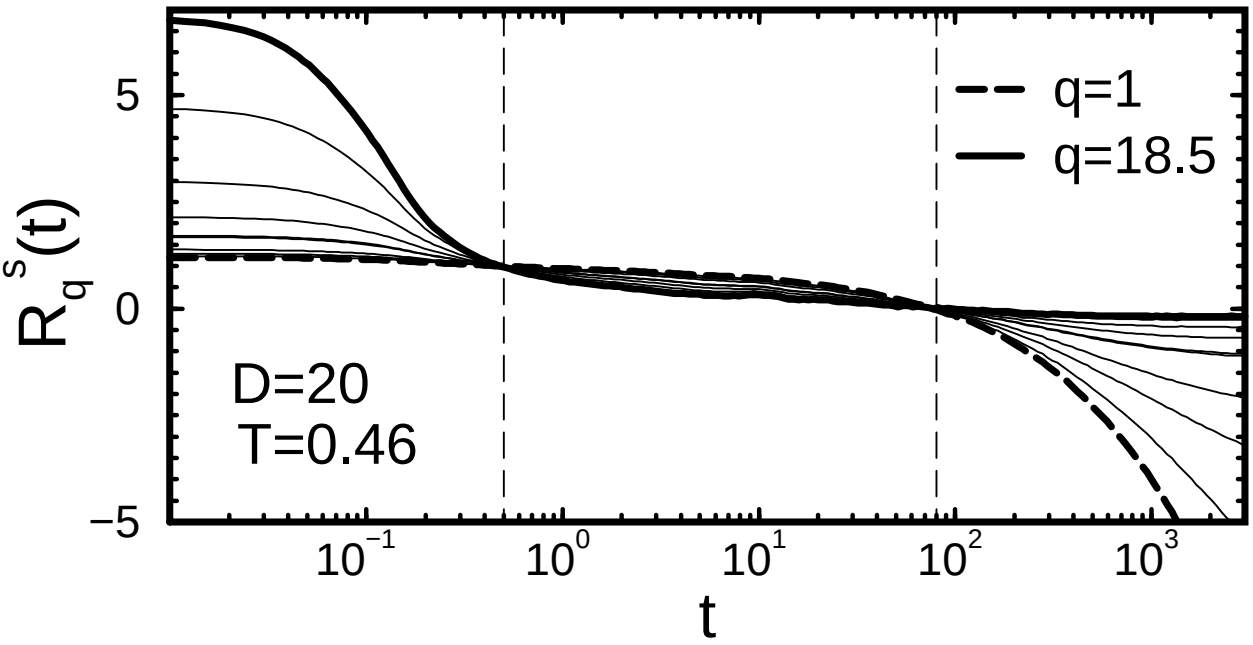
q=1
q=18.5
D=20
T=0.46
$R_q^s(t)$
t
5
0
−5
10^{-1}
10^0
10^1
10^2
10^3

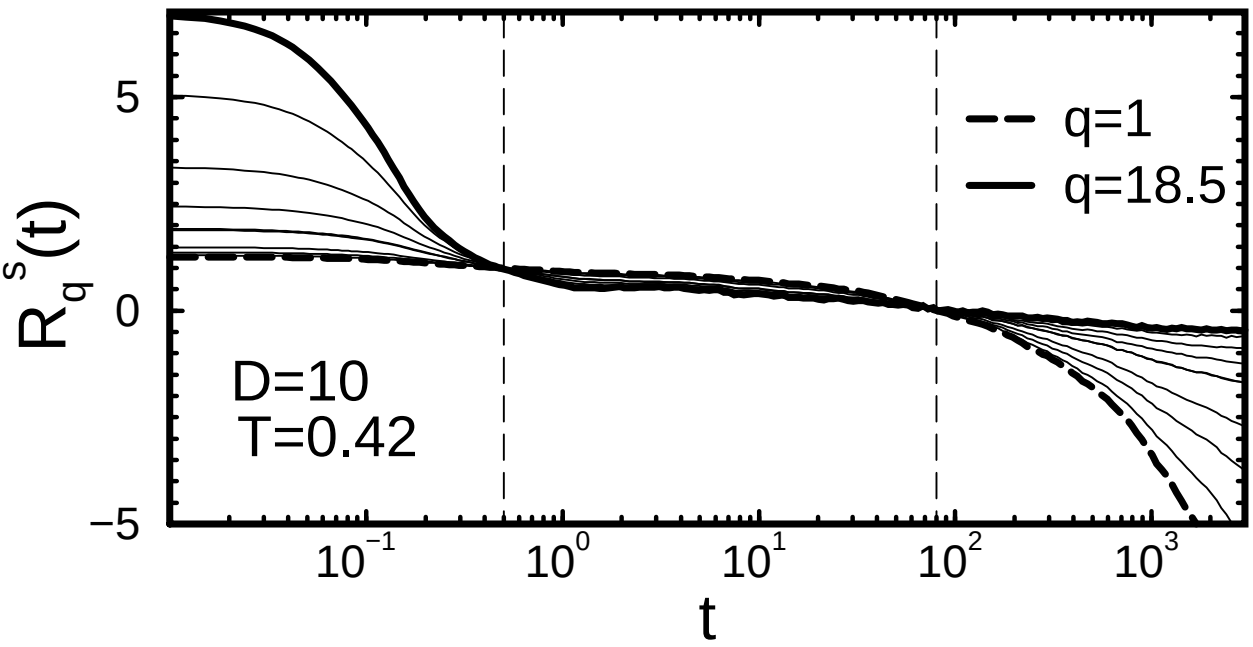
5
0
−5
$R_q^s(t)$
D=10
T=0.42
q=1
q=18.5
10^{-1}
10^0
10^1
10^2
10^3
t

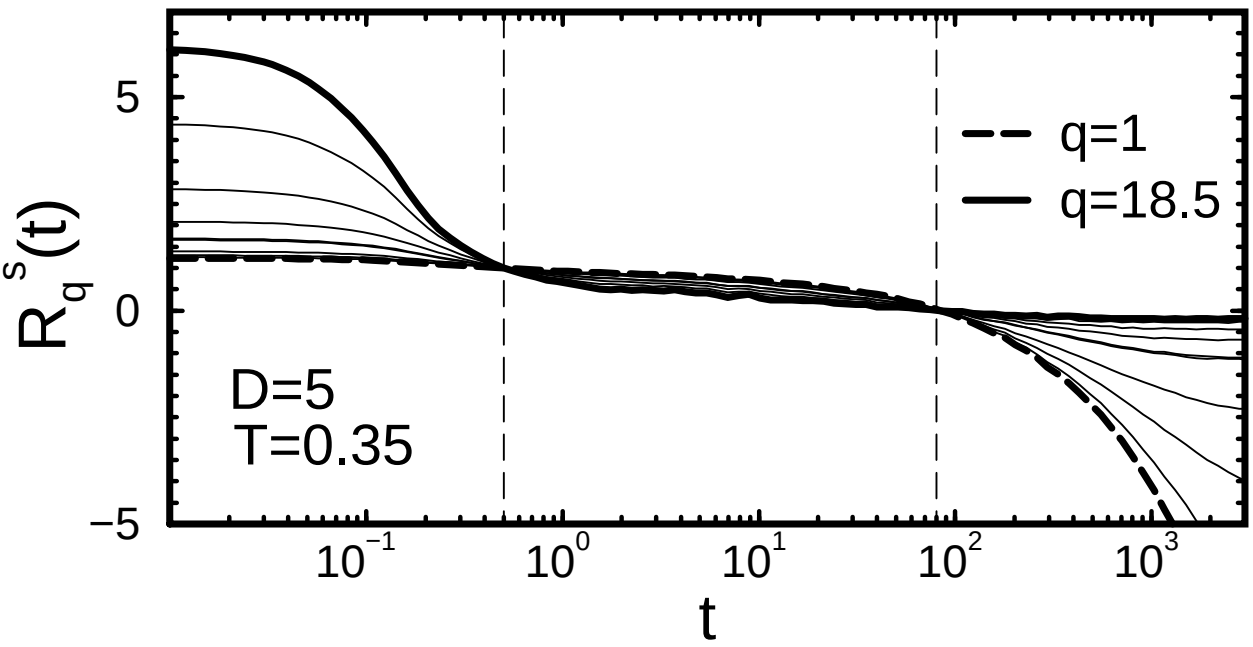
5
0
−5
$R_q^s(t)$
D=5
T=0.35
q=1
q=18.5
10^{-1}
10^0
10^1
10^2
10^3
t

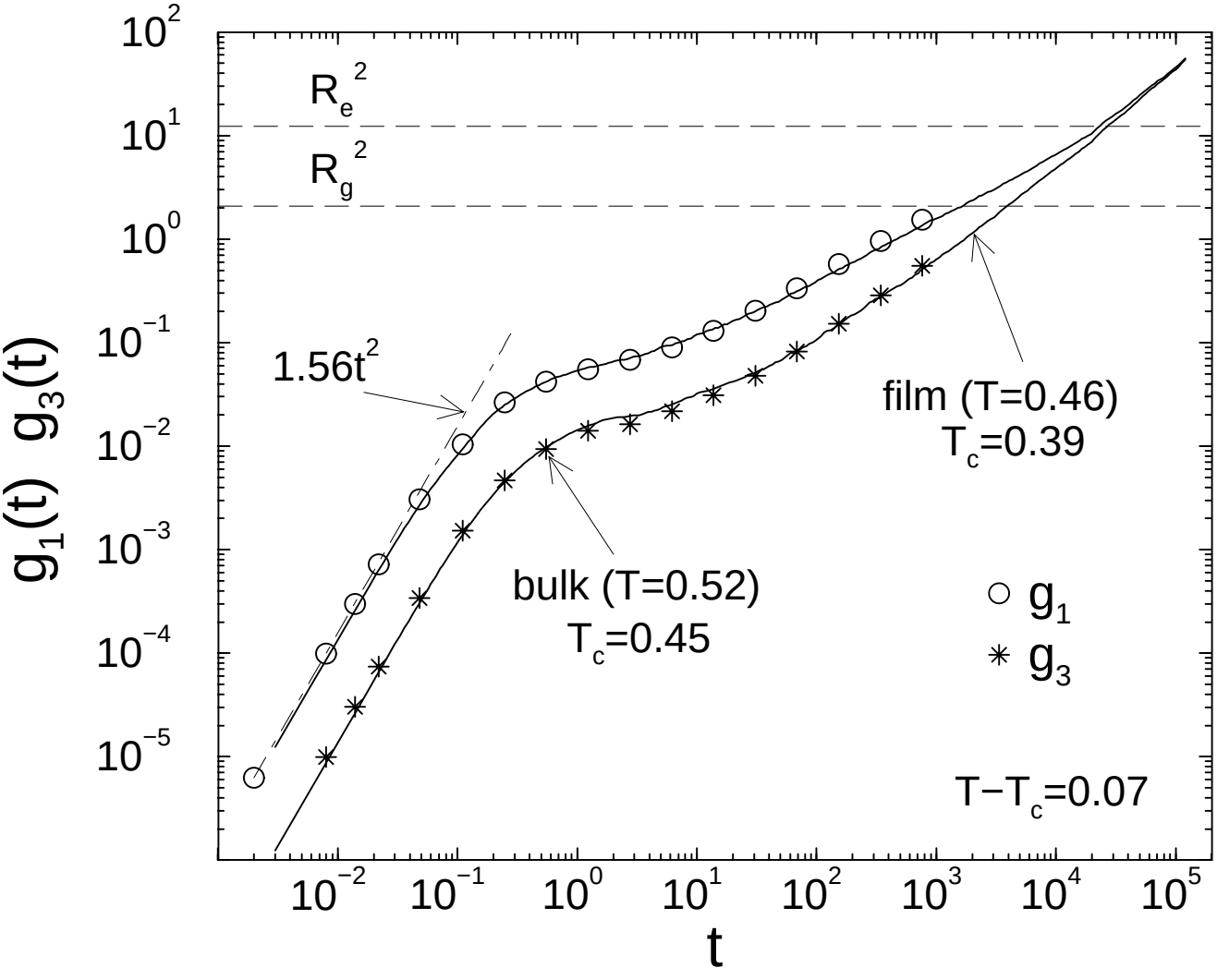
10^2
10^1
10^0
10^{-1}
10^{-2}
10^{-3}
10^{-4}
10^{-5}
$g_1(t)$ $g_3(t)$
R_e^2
R_g^2
$1.56t^2$
film (T=0.46)
T_c=0.39
bulk (T=0.52)
T_c=0.45
g_1
g_3
$T-T_c$=0.07
10^{-2} 10^{-1} 10^0 10^1 10^2 10^3 10^4 10^5
t

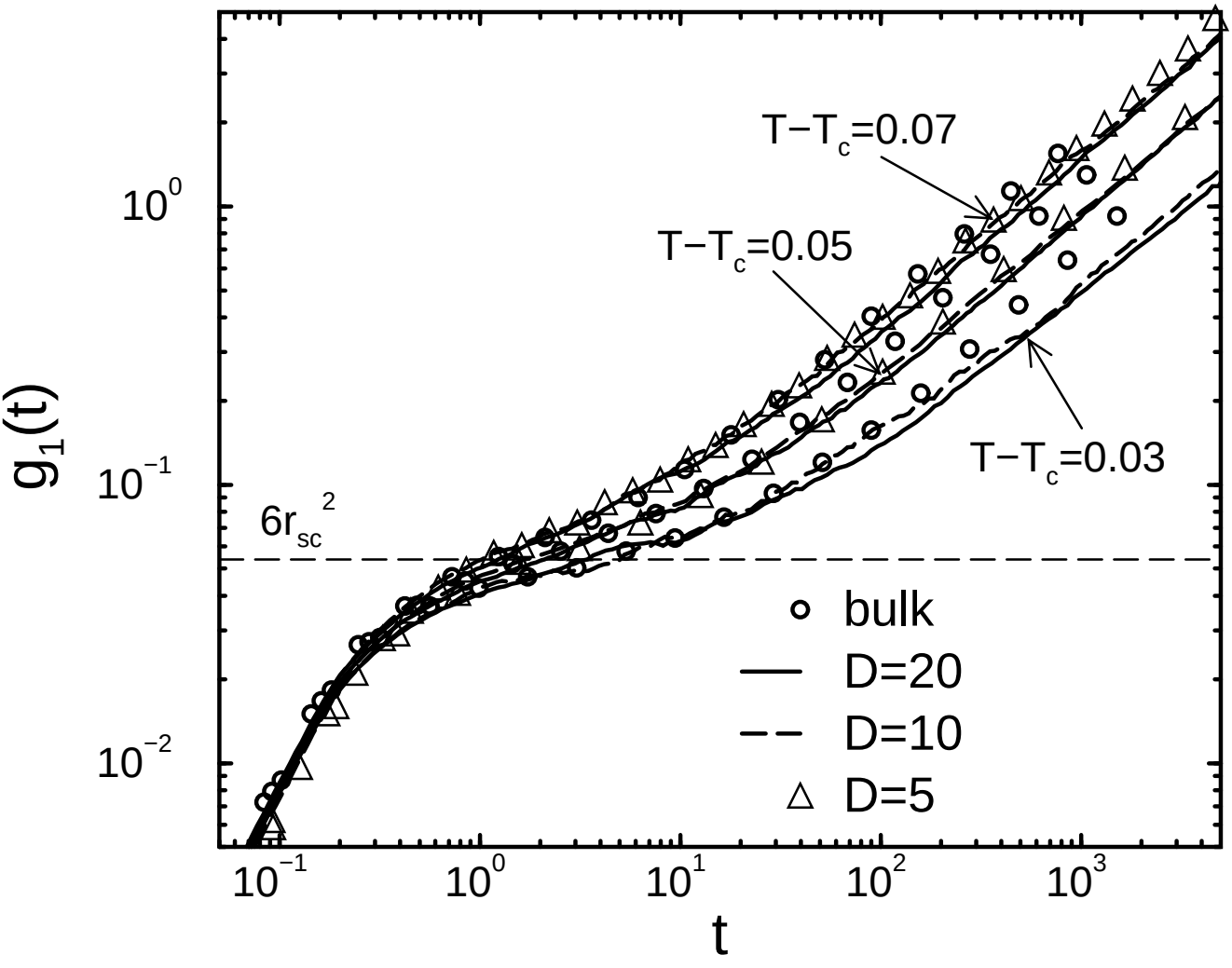
$g_1(t)$
10^0
10^{-1}
10^{-2}
$6r_{sc}^2$
$T-T_c=0.07$
$T-T_c=0.05$
$T-T_c=0.03$
bulk
D=20
D=10
D=5
10^{-1}
10^0
10^1
10^2
10^3
t

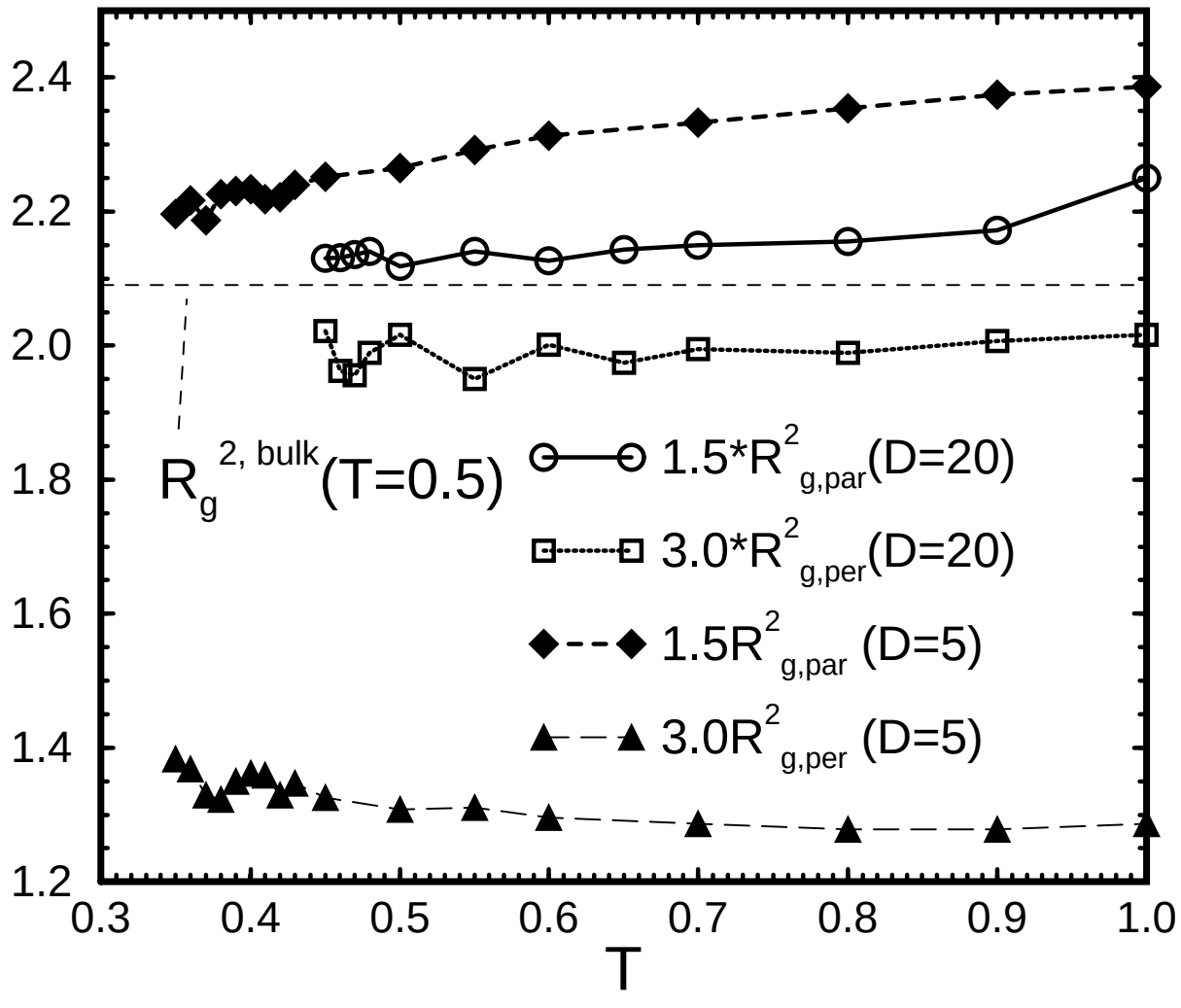
2.4
2.2
2.0
1.8
1.6
1.4
1.2
0.3
0.4
0.5
0.6
0.7
0.8
0.9
1.0
T
R_g^2, bulk(T=0.5)
1.5*R^2_g,par(D=20)
3.0*R^2_g,per(D=20)
1.5R^2_g,par (D=5)
3.0R^2_g,per (D=5)

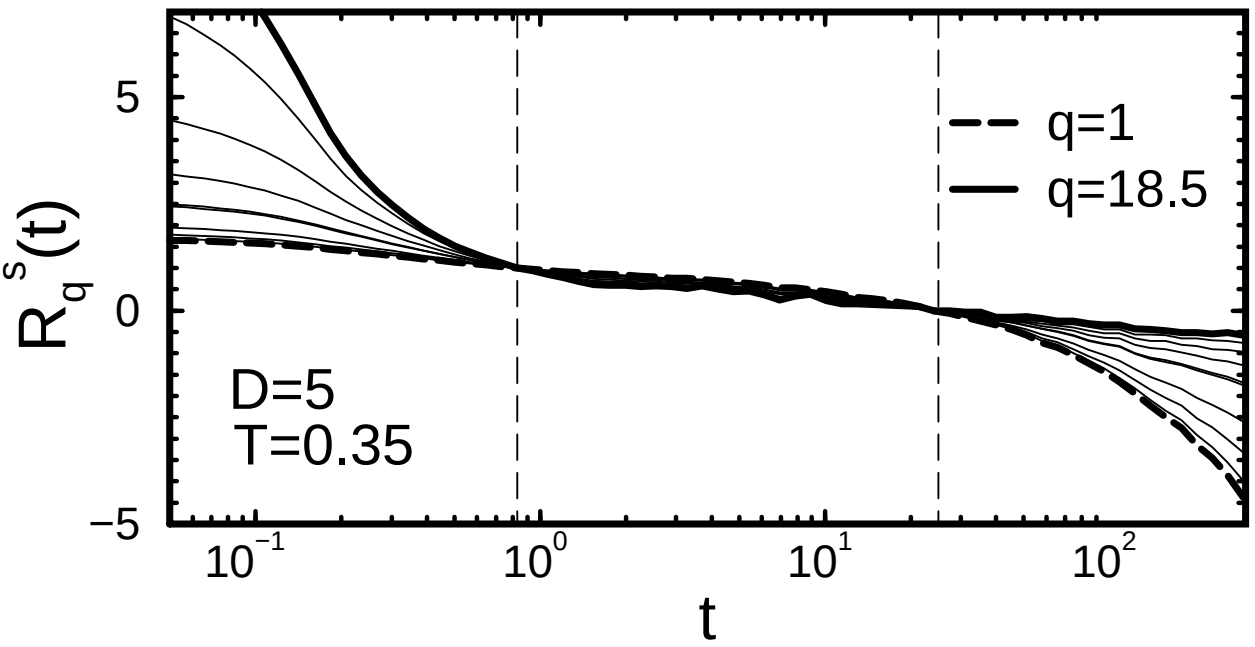
5
0
−5
$R_q^s(t)$
D=5
T=0.35
q=1
q=18.5
10^{-1}
10^{0}
10^{1}
10^{2}
t

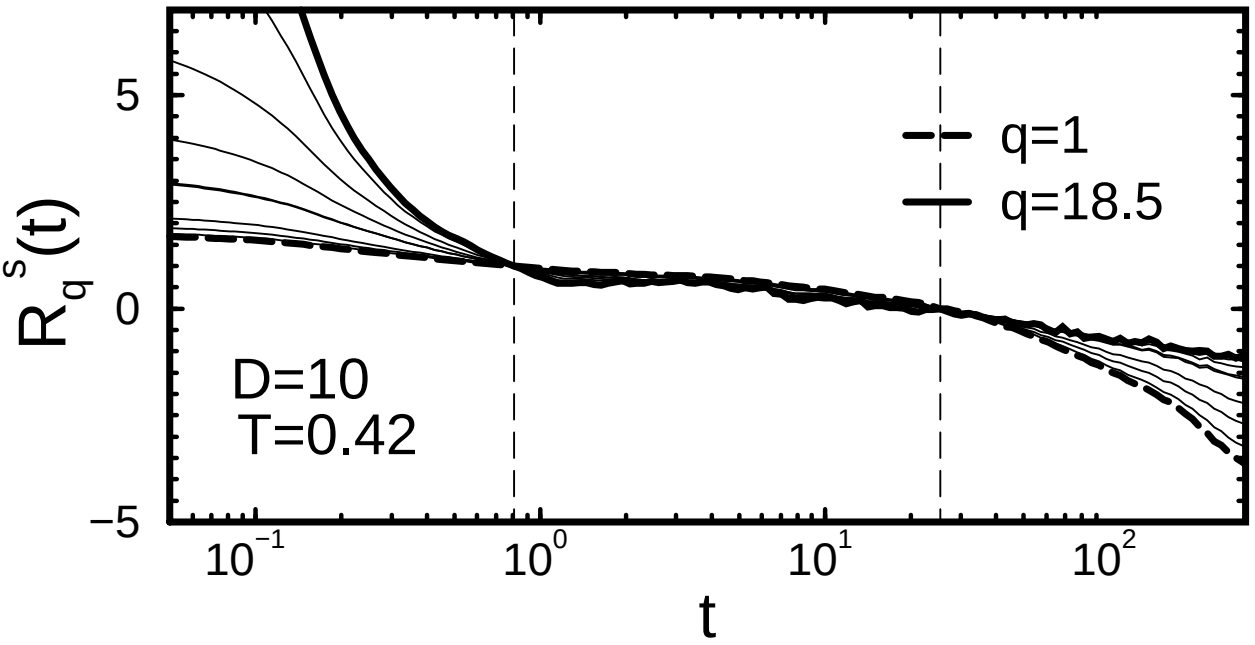
5
0
−5
$R_q^s(t)$
q=1
q=18.5
D=10
T=0.42
10^{-1}
10^0
10^1
10^2
t

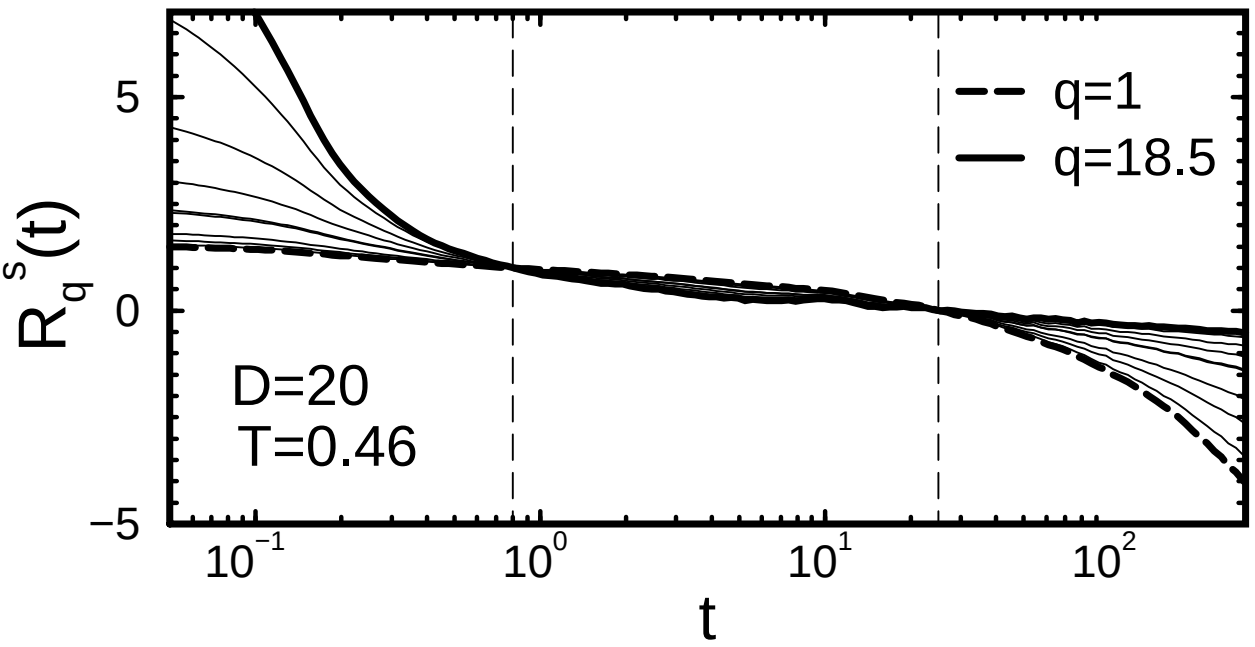
q=1
q=18.5
D=20
T=0.46
$R_q^s(t)$
t
5
0
−5
10^{-1}
10^0
10^1
10^2